3

INVESTIGATION OF ENERGETIC ELECTRON INTENSITIES IN THE EARTH'S OUTER RADIATION ZONE WITH OGO 1[*]

6

by

6 H. Kent Hills[**] 7

7- R 9

A thesis submitted in partial fulfillment of the
requirements for the degree of Doctor of Philosophy
in the Department of Physics and Astronomy
in the Graduate College of
The University of Iowa

9 August, 1967 11

Thesis supervisor: Assistant Professor Louis A. Frank

---

[*] Research supported in part by the National Aeronautics and Space Administration under Contract NAS5-2054.

2

[**] Graduate Research Fellow of the National Aeronautics and Space Administration during the period 1962 through 1965.

ACKNOWLEDGMENTS

I wish to thank Dr. L. A. Frank for his advice and guidance during the course of this work. I also thank Dr. J. A. Van Allen for his continuing encouragement and support. The work of these two in the design of the equipment and in the supervision of the project is gratefully acknowledged.

Thanks are due also to the many others at the University of Iowa who helped in the preparation of the equipment and in the computer processing of the data. The contributions of the OGO 1 project personnel of Goddard Space Flight Center are also acknowledged.

ABSTRACT

Observations of intensities of outer zone electrons obtained with University of Iowa instrumentation borne on the earth-satellite OGO 1 during the period September through December, 1964, are presented. Omnidirectional intensities near the magnetic equatorial plane are given for electrons of energy $E > 40$ keV, $E > 130$ keV, and $E > 2$ MeV, and are characterized by short-term variations superimposed upon an over-all long-term decrease. The pitch angle distributions of electrons ($E > 40$ keV and $E > 130$ keV) may be approximated by the function $\sin^n \alpha$ with n generally found to be less than or about unity throughout the outer zone ($3 \lesssim L \lesssim 7$). Computations of the effects of geomagnetic storms upon the distribution of intensities of these electrons with energies above the detector thresholds are summarized. These results are compared with observations in order to distinguish between adiabatic and non-adiabatic particle behavior. Adiabatic motions are shown to be capable of causing large temporal variations in electron intensities during a magnetic storm.

TABLE OF CONTENTS

LIST OF TABLES

I. INTRODUCTION

The gross nature of the charged-particle population of the geomagnetic field has been firmly established with in situ observations with a large number of rocket-and satellite-borne instruments during the past several years. Farley [1963], Frank and Van Allen [1964], Hess et al. [1965], and Shabansky [1965] have presented comprehensive reviews of observations and theoretical results. Early theoretical work on the trajectories of charged particles in a dipole field was carried out by Stormer [1955], while Alfven [1950] introduced the guiding center approximation of charged particle motion, in which the particle motion is separated into three fundamental motions with characteristic time scales. The particle gyrates rapidly around its guiding center, while the guiding center oscillates in latitude and drifts slowly in longitude. Northrop and Teller [1960] and Northrop [1963] have developed further the theory of the adiabatic invariants of charged particle motion. This theory explains well the basic particle behavior, as is illustrated by the success of the L parameter of McIlwain [1961], which eliminates to a large degree the longitude of an observation as an important coordinate.

Although L loses some of its original significance at large values of L ($L \gtrsim 6$), it remains a good ordering parameter for observational data and provides a reference coordinate for observations of charged particles moving in the geomagnetic field.

The present investigation utilizes data obtained with the University of Iowa detectors borne on the earth-satellite OGO 1. The intensities of electrons of energies above 40 keV, above 130 keV, and above 2 MeV are presented herein for L=2.5 to 9 for the period from launch in early September, 1964 through December 31, 1964, a period near the minimum of the solar activity cycle. The electron intensities near the magnetic equator are characterized by short-time (~ days) variations superimposed upon a general decline of intensities throughout this period. The observations will be compared with the results of computations based on conservation of the adiabatic invariants in an attempt to distinguish between adiabatic and non-adiabatic fluctuations.

Early suggestions for possible sources of the observed zones of trapped particles included mechanisms involving a violation of at least one of the adiabatic invariants. Theoretical treatments of diffusion processes were given by Kellogg [1959], Herlofson [1960], Parker [1960], and Davis and Chang [1962]. The latter two investigations considered the fast approach of an infinitely-conducting plane (Chapman-Ferraro model) and its subsequent slow withdrawal. The motion of trapped charged particles was calculated and a net radial displacement was predicted. Such diffusion was observed by Frank [1965a] and by Craven [1966]. The work of Nakada et al. [1965] considered particles trapped in a dipole field and investigated the consequences of the violation of the third invariant only, but without specifying any particular mechanism leading to the violation (i.e., leading to a radial displacement of the particles). Their results for the variations of intensity with pitch angle and L agreed with observations of 0.1 to 5 MeV protons in the outer zone. Similarly, Nakada and Mead [1965] considered the diffusion produced by temporal variations in the deformation of the magnetosphere by the solar wind. Tverskoy [1964, 1965] has also computed the effects of magnetic field fluctuations. Taylor [1966] considered adiabatic motions of outer zone particles in model fields of the earth, and recently, Roederer [1967] considered the adiabatic motions of charged particles in an asymmetric model magnetosphere. Dessler and Karplus [1961] considered the changes in the magnetic field which were due to a model ring current and calculated the effects of betatron acceleration for that model, in terms of particle relocation and energization, conserving all three of the adiabatic invariants. Coleman [1961] calculated the effects of betatron acceleration on relativistic particles which experience a slow change in magnetic field strength.

Numerous observations have been reported of the large effects of magnetic storms on charged particle intensities in the outer radiation zone [Farley and Rosen, 1960; Forbush et al., 1962; Frank et al., 1964; Craven, 1966; and McIlwain, 1966b]. McIlwain [1966a] has demonstrated that measured short-term proton intensity variations at $L < 2.4$ were in agreement with predictions computed by conserving all three adiabatic invariants, using a simple magnetic field disturbance model. Recently, the fluctuating intensities of outer zone electrons ($E > 0.5$ MeV) were shown by McIlwain [1966b] to have adiabatic components which were closely related to $D_{ST}(H)$. Whereas Dessler and Karplus [1961] used a disturbance magnetic field calculated from a model ring current, McIlwain's computations [1966a] for the inner zone used a disturbance field constant over low radial distances ($L < 2.4$). The present adiabatic motion computations, which give the combined effects on the counting rate of a detector with given energy threshold, also conserve all three invariants, and utilize a model disturbance field patterned after the satellite measurements which Cahill [1966] reported for the period of the geomagnetic storm of April 17, 1965. The magnitude of the model disturbance field was taken to be proportional to $D_{ST}(H)$, the average equatorial storm disturbance of the H component of the magnetic field measured at the surface of the earth (see Sugiura [1964] for the method of derivation of $D_{ST}(H)$). The recent report by Frank [1967] of the discovery of the charged particles of the extraterrestrial ring current during geomagnetic storms provides additional information on the strength and location of the ring current and the resulting magnetic field disturbance.

The temporal variations of electron intensities by factors of 10-100 in the outer zone observed with OGO 1 in late 1964 near solar minimum were similar to those observed by many other workers during other periods [Forbush et al., 1962; Frank et al., 1964; Frank, 1966; Armstrong, 1965; Brown and Roberts, 1966; and Williams, 1966], although the slot was located at larger L-values during solar minimum [Frank and Van Allen, 1966]. An example of the relation of the structure of the trapping region to the rest of the magnetosphere was obtained with the observation of a sudden decrease in intensities of energetic electrons in the trapping region, observable down as deep at $L \sim 5$, coinciding with a compression of the shock boundary observed by other instruments. The OGO 1 results reported herein include information on pitch angle distributions as well as omnidirectional intensities. The spacecraft was spinning, which caused a spin modulation of the counting rates of the directional detectors. The modulation patterns observed below $L \sim 8$ were consistent with pitch angle distributions of the form $j(\alpha) \propto \sin^n \alpha$. Relatively isotropic fluxes, at least over the range of directions within 40° of the plane perpendicular to the field, have been previously observed in the outer zone [Fan et al., 1961; Farley and Sanders, 1962; Pfitzer et al., 1966; Pizzella et al., 1966; and Serlemitsos, 1966], and the consistently low values of n determined here from the observed spin modulation confirm that this is a persistent feature of the angular distributions of outer zone energetic electrons.

II. DESCRIPTION OF THE APPARATUS

This investigation utilizes data from the University of Iowa detectors on board the satellite OGO 1, which was launched on September 5, 1964. Only data obtained from launch until December 31, 1964, are included in this study. The spacecraft orbit is inclined 31° to the equatorial plane, with a 64-hour period and initial apogee and perigee of 155,000 km and 6600 km geocentric radial distances, respectively. Apogee was initially located on the evening side of the magnetosphere and progressed to midmorning by the end of December, 1964, as shown in Figure 1, which shows the projection of the orbit onto the solar ecliptic equatorial plane. Figure 2 shows the projection of the orbit onto the solar ecliptic meridional plane passing through the apogee position. As shown in the figure, the spacecraft reaches a maximum distance of 9.5 R_E (earth radii) above the ecliptic plane, at a point where the radial distance projected onto the ecliptic plane is 22 R_E. The path of the spacecraft with respect to the geomagnetic equatorial plane varies with the rotation of the earth, so that even at large radial distances the orbit may lie near the equatorial plane on inbound passes, and magnetic latitudes as high as about 45° may be reached on outbound passes.

Figure 3 shows a diagram of the detector array, which consists of three pairs of Eon type 6213 directional Geiger-Mueller detectors (denoted by A1 and B1; A2 and B2; and A3 and B3), an Anton type 302 omnidirectional GM detector (denoted by C), and a two-channel directional PN junction proton detector (denoted by H). The directional detector apertures are flush with the surface of the 8 inch diameter spherical shell of the experiment package, while the omnidirectional detector is mounted in a housing projecting about two inches outside of this spherical shell. The type 6213 detectors nominally have 1.2 mg/cm^2 mica windows. Those designated by "A" are unshielded, while those designated by "B" are shielded by an additional 10.2 mg/cm^2 of aluminum. The fields of view of the A and the B detectors are conical, with half-angles of 45°, within which electrons are efficiently detected by A for energies $E > 40$ keV, and by B for energies $E > 130$ keV. Outside of this field of view the detectors are shielded by lead and other material. Detector C efficiently detects electrons of energies $E \gtrsim 2$ MeV. The GM detectors are sensitive to protons as well as to electrons, while the PN junction detector, prepared by R. Walker Fillius, is sensitive to protons of energies within its two channels, but has negligible sensitivity to electrons.

The proton energy thresholds are 500 keV and 910 keV, the former also being the nominal proton energy threshold of the type "A" GM tubes. Hence, the proton detector responses may be used to eliminate the proton contribution to the GM tube counting rates. No other application of the proton measurements is reported in this paper. The shielding and geometric factors of the detectors are given in Table 1. Appendix I summarizes the detection efficiency as a function of electron energy for the GM detectors. The calculation of the geometric factors, which depend on the angular distribution of the incident particle intensities, is described in Appendix II. Appendix III includes a summary of the dead-time corrections which must be made to the observed GM detector counting rates and of the temperature dependences. Temperature effects are small and dead-time corrections are negligible at telemetered counting rates below about 10^3 counts/second, typically.

The planned spacecraft attitude control was not achieved, due to boom deployment failure, but the satellite was spin-stabilized at 5 r.p.m. with the spin vector aligned within a few degrees of the spacecraft body Z-axis and directed approximately at celestial coordinates 45° right ascension and -8° declination.

Table 1

Detector Characteristics

Description	A1	B2	C	H*
Detector	EON 6213		Anton 302	Ortec p-n junction
Viewing angle	cone: 45° half-angle		~ 3π sr	π/2 sr
Shielding				
Window, mg cm^{-2}	1.2 mica	1.2 mica 10.2 aluminum		0.2 nickel
Wall, g cm^{-2}	0.4 stainless steel 0.2 lead 0.2 other material		0.4 stainless steel 0.51 other material	
Penetration energy				
Window	$E_e \sim 40$ keV $E_p \sim 745$ keV	$E_e \sim 130$ keV $E_p \sim 2.1$ MeV		Insensitive to electrons E_p = 500 keV and 910 keV
Wall	$E_e \sim 5.5$ MeV $E_p \sim 35$ MeV		$E_e \sim 2$ MeV $E_p \sim 24$ MeV	
Geometric factor				
Directional, εg, $cm^2 sr$	2.9×10^{-3}**	2.1×10^{-2}**		0.011
Omnidirectional, εG, cm^2			0.1***	

* R. W. Fillius [private memorandum, 1965].

** For isotropic flux. See Appendix II.

*** Dependent upon energy spectrum. See Appendix II.

The orientation failure resulted in the telemetry antenna pointing away from, rather than toward, the earth during most of each orbit. However, reasonable coverage over an orbit was provided by real-time telemetry reception plus the use of the onboard tape recorder, which could store about 24 hours of data at low bit rate (1000 bps). At low bit rate, a given detector is sampled once every 9.216 seconds, with an accumulation period of 1.142 seconds. At medium (8,000 bps) and high (64,000 bps) bit rates, these system times become 1/8 and 1/64, respectively, of the values for the low bit rate. The proton detector incorporates a subcommutator which alternately samples its two energy channels, so that each proton channel is sampled only half as frequently as each of the GM detectors.

The three pairs of directional GM tubes are mutually orthogonal, with the proton detector parallel to A1 and B1. The arrangement is such that each of these detectors is directed at an angle of 54.7° to the spacecraft Z axis, as illustrated in Figure 3, where the Z axis is normal to and directed out of the plane of the paper. Thus, all of the directional detectors are directed at an angle of about 55° to the spin vector, so they all follow approximately the same path in celestial coordinates while the spacecraft spins. Figure 4 shows the path of the center of the field of view of detectors A1, B1, and H during the 12-second spin period. The paths of the other detectors lie within 3° of this path. The sun does not come near this path during the last four months of the year, so none of these detectors can view the sun, even at the extreme edge of the field of view, during the time period covered here.

The experimenters' data, supplied to the University of Iowa by the NASA Goddard Space Flight Center, consist of counting rates, various housekeeping parameters, the Universal Time assigned to each record, and the reading of the spacecraft clock, which is incremented once each second. The orbit data are furnished separately, and are merged with the detector counting rates at the University of Iowa. The attitude of the spacecraft, i.e., its azimuthal orientation about its spin axis, can be determined from the responses of the solar cell arrays, but for the present observations only the location in orbit is generally known, and not the attitude. For selected time periods attitude information is available, but use of it was restricted herein to a few passes where the spin modulation of the detector responses was investigated in detail. For such periods, the basic information includes the celestial coordinates of the spacecraft body axes at specified times. The directions of the fields of view of the GM tubes are determined for these times, and appropriate rotations about the spacecraft spin axis are carried out to yield the detector directions in celestial coordinates at each second of time for which there are counting rate data. For most of the observations of directional intensities reported here, it is sufficient to know only the angle between the local magnetic field and the spin axis. See Appendix II for details.

Observations during a low-latitude inbound pass of the spacecraft on October 17, 1964 are displayed in Figure 5, which is a machine plot of the observed counting rates as functions of geocentric radial distance. Some general features characteristic of our observations can be seen here. Note (a) the high inner zone counting rates, particularly of detector C; (b) the "slot", which lies farther out for lower energy particles; and (c) the abrupt cut-off in the counting rates at the edge of the region of durable trapping (at L ~ 12, radial distance ~ 75,000 km here), with quite variable rates outside this region, and a smooth structure just inside. Note also the spikes of high intensities (at about 97,000 and 110,000 km) which are found out to quite large radial distances, rising above the low intensities generally observed at large distances. The counting rate modulation due to the spacecraft spin is easily noted in the trace of the counting rates of the directional detectors and variations in the modulation are also seen, notably the broad minimum through the outer zone, and an increase near the boundary of stable trapping. The modulation period which appears in the plot at about 20,000 km in H1 and H2 is not the actual period, but rather is due to the detector sampling schedules employed by the spacecraft data system and by the machine plot program, which does not plot every point. The spin modulation effects are discussed in detail in Appendix II. The base lines appearing in Figure 5 correspond to 1 count per frame, and frame counts of both zero and one are plotted at this level.

III. OBSERVATIONS IN THE OUTER RADIATION ZONE

3.1 Angular Distributions of Electron Intensities

The directional detectors A1 and B2 sample particle intensities over a wide range of local pitch angles as the spacecraft spins, as discussed in Appendix II and illustrated in Figure 25. The detectors have quite wide (45° half-angle) collimator fields of view, and the detector response to a well-collimated beam of particles depends upon the angle of incidence of the beam, decreasing by a factor of two as the beam moves from the center of the collimator to an angle about 30° away from the center. The pitch angle distributions have been approximated by a $\sin^n\alpha$ fit in order to characterize the observed distributions by appropriate values of n determined (see Appendix II) from the observed spin modulation of the counting rates. The actual pitch angle distribution is not expected to be well described by $\sin^n\alpha$ at small angles α, but n does provide a consistent parameter for description of the general character of the angular distributions of particle intensities.

The values of n obtained from the data from detector A1 were similar to those obtained from detector B2 data, and both were plotted vs L for each pass of the spacecraft through the radiation zones. A representative machine plot of this type is shown in Figure 6, where ENA and ENB denote the values of n obtained from the data from detectors A1 and B2 respectively. The values of ENA and ENB are reliable when Γ (also shown) is $\gtrsim 15°$ The maximum true counting rate RA of detector A1 in the spin cycle is also shown for reference. The energy spectrum indices also on this plot will be discussed below.

The form of the angular distribution displays little temporal variation, and through most of the outer zone, from $L \sim 3.5$ to $L \sim 7$, the angular distribution of electron ($E > 40$ keV and $E > 130$ keV) intensities can be characterized by $n \sim 0.7 - 1$, indicating that the distribution is relatively isotropic, at least over the range of angles within about 40° of perpendicular to the field. This result is in good agreement with the report made by Pfitzer et al. [1966] of angular distributions also observed on OGO 1 for two representative passes, and with the observations of Pizzella et al. [1966] and of Fan et al. [1961]. Serlemitsos [1966] noted the approximate isotropy in the outer zone and showed the occasional departure from isotropy, at distances greater than 7 or 8 R_E, with angular distributions peaked parallel to the field. The OGO 1 results have confirmed the existence of such distributions peaked along the field on several occasions [Hills, 1967], but these occurred at large L, out to 14, and are not discussed here. The persistently low values of n indicate that corrections of observed intensities for dependence on latitude (i.e., B/B_o) can be done without imposing extremely large corrections to convert the intensities to equatorial values.

The increases in ENA and ENB seen in Figure 6 below $L \sim 3$ illustrate the fairly sharp change in character from the approximately isotropic outer zone to the inner zone, which is well-known to have steep angular distributions, and where ENA and ENB become 20 and larger (all $n > 20$ are plotted as 20 in Figure 6). Figure 6 also shows the two-point integral energy spectrum indices ABN, ACN, and BCN, for a spectrum of the form $j(> E) \propto E^{-N}$. The first two letters in the index labels indicate the two detectors used for the determination of the index. The rapid (spatial) spectral variations near $L = 3$ are reflections of the slot as seen by the different detectors. ABN and ACN are too high for $L \lesssim 3.5$ since the contributions of protons to the counting rates of detectors A1 and B2 have not been removed here. The general character is a progressively softer (higher N) spectrum as L increases above 4 or 5, with median values of ABN ~ 1.5 at L = 5 and ~ 3.5 at L = 9.

3.2 Omnidirectional Intensities of Electrons

Omnidirectional intensities have been obtained from 5-minute averages of the detector counting rates, as discussed in Appendix II, and have been plotted as a function of L for each pass. These intensities were then corrected to equatorial values using the dependence on the magnetic field strength ratio B/B_o as outlined by Frank and Van Allen [1963]. If the directional intensity of particles at the equator is given by $j(\alpha_o) \propto \sin^n \alpha_o$, then at any point on the same line of force the omnidirectional intensity dependence on B/B_o is given by $J(B/B_o) \propto (B/B_o)^{-n/2}$. Each pair of consecutive inbound-outbound passes of the spacecraft through the outer zone provided the intensities at two different values of B/B_o on each L shell. The observed dependence of omnidirectional intensity obtained from these pairs of data points was approximated by $(B/B_o)^{-x}$ with $x \sim 0.7$ for detector C and $x \sim 0.4$ for detectors A1 and B2. This is consistent with the values $n \sim 0.7 - 0.8$ determined from the $\sin^n \alpha$ fit to the angular distributions of intensity measured by the directional detectors A1 and B2. Thus the correction of measured omnidirectional intensities to equatorial values was carried out according to $J \propto (B/B_o)^{-n/2}$ with $n/2 = 0.4$ for the intensities measured by detectors A1 and B2 and $n/2 = 0.7$ for the intensities measured by detector C. Proton contributions to the counting rates of the detectors were eliminated, utilizing the PN junction detector data. There was no correction needed to the counting rates of detector C, and the corrections for detectors A1 and B2 were nil for $L \gtrsim 4$. For lesser L-values the maximum correction to the detector B2 counting rate was typically a decrease by $\lesssim 20\%$ and the maximum correction to the counting rate of detector A1 was typically a decrease by $\lesssim 50\%$. The corrected intensity plots were used to construct contours in an (L, time) space of constant intensity of electrons of energies $E > 40$ keV, > 130 keV, and > 2 MeV. These contours are shown in Figures 7, 8, and 9 respectively, along with the 2-day average of the daily sums of the geomagnetic index K_p. There is a gross correlation between the occurrence of K_p peaks and of enhanced intensities in the outer zone of electrons in the ranges of energy $E > 40$ keV and $E > 130$ keV, while for electrons ($E > 2$ MeV), the enhancement seems to lag behind the K_p increases by a few days. The intensities near the "slot" are relatively steady for electrons ($E > 2$ MeV) at $L \sim 3$, but variable for electrons ($E > 40$ keV and $E > 130$ keV), for which the "slot" location itself is variable ($L \sim 3.5$ for $E > 40$ keV, $L \sim 4$ for $E > 130$ keV). The cross-hatched lines in Figures 7-9 denote the location of the minimum intensity (the "slot").

Note that on 15 September, when the intensities measured by detectors A1 and B2 in the outer zone were highest, these intensities increased greatly at low L-values as well as in the heart of the outer zone, while the intensities seen by detector C at low L-values remained relatively constant. The steeper gradients of the intensities of the higher energy electrons are responsible for the fact that the detector C contour plot is more easily readable than the plot of the detector A contours. On October 17 and November 15 there were detected marked reversible apparent compressions of the outer magnetosphere, with the detector C contour of 10 counts/sec, for example, moving in from $L \sim 8.5$ to $L \sim 6.5$ in the first case and from $L \sim 9$ to $L \sim 7$ in the second. With a plasma experiment also on OGO 1, Binsack and Vasyliunas [1967] detected similar compressions of the shock boundary, reporting that during the event of November 15 the shock boundary was found at a radial distance of 85% of its usual distance, in agreement with expectations based on simultaneous IMP 1 measurements of the dynamic plasma pressure in the interplanetary medium.

It can be seen in Figure 9 that the effects of the November 15 event were significant at least as far in as $L = 4$ for electrons of energy above 2 MeV. Lack of data prevents a more precise determination of the lowest L shells affected. The phenomenon observed here actually involved a sudden loss and subsequent replenishment of electrons of energies $E > 40$ keV, $E > 130$ keV, and $E > 2$ MeV, since the intensities did not increase at lower L-values, as would happen if the electrons were transported inward with no losses of energy or intensity. The decreased intensities of electrons of energies greater than 2 MeV were first seen at large L-values on the inbound pass of November 15, and intensities were decreased at all L-values down to $L \sim 5$. No data were available for $L < 5$ on this pass. On the following outbound pass data were available for $L \gtrsim 3.6$, and the intensity decrease was seen at $L \gtrsim 4$. At $L = 5.8$ the intensity was about the same as it had been on the inbound pass, but by the time $L = 9$ was reached (about 7 hours after the inbound pass at the same L), the intensity there had returned nearly to its pre-event value. However, the recovery at low $L(\sim 5)$ did not occur until some 5 days later.

The shock boundary compression observed by Binsack and Vasyliunas on October 26 did not show any clearly noticeable effects on the intensities of the electrons investigated here. The October 17 event evident in Figure 9 is similar to that of November 15, except that the disturbance appears to have a lesser effect on the intensity near L = 5, and, in fact, did not appear much below L = 5. The apparent event (or series of events) near September 18 is of a completely different character. In this case the intensities of electrons in the two lower energy ranges vary in much the same way as during the October 17 event, but the intensities of electrons ($E > 2$ MeV) display marked differences. The September event evolves on a longer time scale, with a general intensity decrease at L-values above about 3. The location of the maximum of intensity of electrons ($E > 2$ MeV) moves inward while the peak intensity declines for about a week. Subsequently, a well-defined peak of intensity rises at $L \sim 4.8$, returning the intensities in the outer zone to a spatial structure similar to that existing on September 15 before the event, but with a factor of about 10 decrease in intensity levels.

The data displayed in Figures 7, 8, and 9, reorganized by putting together data for all three detectors at one L shell, are given in Figures 10, 11, and 12 for L = 3, 5, and 7, respectively. The marked compressions discussed above are particularly apparent at L = 7, but can also be found at L = 5. The characteristic feature of the intensities shown in these three figures is the superposition of short-term (~ days) variations, both increasing and decreasing, upon a general long-term decline, concurrent with a general decline in the K_p daily sum. The 64-hour period of the satellite, of course, allows some short-time variations to be only partially resolved, or not at all. A local time variation of intensity at a given L would appear here as a long-term variation, due to the orbital motion of the spacecraft, but Frank [1966b] has shown that for intensities of electrons of energy greater than 1.6 MeV, there is little local time effect below L ~ 6, and Williams and Palmer [1965] have shown only a slightly asymmetry at L ~ 5 for 280 keV and 1.2 MeV electrons at low altitudes. The data at L = 3 shown in Figure 10 illustrate the relative lack of fluctuations in electron (E > 2 MeV) intensities in the slot, which is at L ~ 3 for this energy at this time. (See [Frank and Van Allen, 1966] for a correlation of the slot location with the solar cycle.)

The evident long-term intensity decline is most pronounced for 2 MeV electrons at L = 5 (Figure 11), indicating a lessening of the outer zone peak intensities while shrinking in the outer edge of the zone only slightly. The large variations in intensity shown here are consistent with the large variations reported in several papers. Variations in intensities by factors of 100 were reported by Frank et al. [1964] for electrons ($E > 1.6$ MeV) measured in 1962-1963 with Explorer 14, and similar variations in intensities were shown by Williams and Smith [1965] for late 1963 at low altitudes. McIlwain [1963] reported the decay of intensities of electrons ($E > 0.5$ MeV and > 5 MeV) at the end of 1962 for L = 3. Intensities declined by a factor of 10 in three months for the 5 MeV electrons, and by a factor of 10 in two months for the 0.5 MeV electrons. Thus, the observed decay presented here is not an unusual feature of the outer radiation zone.

Typical omnidirectional electron intensities at L = 5 at the equator obtained from the present OGO 1 measurements were $\sim 2 \times 10^7$, $\sim 8 \times 10^6$, and $\sim 2 \times 10^4$ cm^{-2} sec^{-1} for electrons ($E > 40$ keV, > 130 keV, and > 2 MeV, respectively). These observations were obtained in the middle of a period of declining intensities near the end of October, 1964, and near solar minimum. At $L = 3$ the electron ($E > 40$ keV, > 130 keV, and > 2 MeV) intensities were $\sim 2 \times 10^7$, $\sim 1.5 \times 10^6$, and $\sim 8 \times 10^2$ cm^{-2} sec^{-1} respectively. These intensities agree closely with the Explorer 14 data (~ 2 years earlier) for electrons of energy above 40 keV, but the OGO 1 intensities of electrons ($E > 2$ MeV) were about a factor of 5 lower than those obtained from Explorer 14 data. Mihalov and White [1966] reported differential electron intensities over the energy range 0.17 to 5.3 MeV measured at high latitudes in August, 1964, with the satellite 1964-45A. Extrapolation of their directional results at large B/B_o to omnidirectional intensities at the equator requires a large and uncertain correction but indicates intensities at $L = 5$ consistent with those reported here. At $L = 3$ the present observations yield intensities of electrons ($E > 2$ MeV) which are lower by a factor of ~ 10 and intensities of electrons ($E > 40$ keV) which are higher by a factor of ~ 10 than those indicated by extrapolation of the high latitude data of August, 1964. The present results are in agreement with the sample differential energy intensities in the heart of the outer zone reported by Pfitzer et al. [1966] for 50 keV to 4 MeV electrons observed also on OGO 1 in 1964, and agree to within a factor of ~ 2 with the electron environment model AE2 ($L \lesssim 6$) of Vette [1965], constructed for the epoch August, 1964.

The electron intensities at high latitudes in the outer zone measured with Injun 4 in December, 1964, through February, 1965 [Frank et al., 1965], were comparatively low ($J_o(> 2$ MeV$) \sim 2 \times 10^2$ cm^{-2} sec^{-1} and $j(> 40$ keV$) \sim 10^2 - 10^3$ cm^{-2} sec^{-1} sr^{-1} at low altitudes in the heart of the outer zone), but the decrease from the earlier intensities observed with Injun 3 [Craven, 1966] and by Mihalov and While [1966] is quite consistent with the presently reported decline of outer zone electron intensities near the equatorial plane. The measurements of McIlwain [1966b] during the period extending from the last few days of 1964 through the middle of August, 1965, yield intensities of electrons ($E > 0.5$ MeV) at $L = 4$-5 which are consistent with the low electron ($E > 2$ MeV) intensities reported here for the end of 1964.

IV. EFFECTS OF ADIABATIC MOTIONS OF CHARGED PARTICLES IN THE OUTER RADIATION ZONE DURING MAGNETIC STORMS

We now compute the adiabatic motions of the trapped charged particles under the influence of given magnetic field fluctuations and investigate the net effect on the observed intensities of electrons ($E > 40$ keV, $E > 130$ keV, and $E > 2$ MeV). Consider particles mirroring at the equator, so that the second adiabatic invariant $I = 0$, and the pitch angle α_o is 90°. In the adiabatic approximation the particles drift in longitude at a radial distance R such that the third adiabatic invariant (flux invariant)

$$\Phi\ (R) \quad = \int_0^{2\pi} \int_0^R B(r)\ r\ dr\ d\varphi = \oint \vec{B} \cdot \vec{ds}$$

is conserved. Here B is the total magnetic field (northward) perpendicular to the equatorial plane, and is composed of a stationary component and a time-varying component, i.e., $B(r) = B_o(r) + \Delta B(r,t)$. Variations in the field on a time scale that is long compared to the longitudinal drift period cause the particles to move to a different radius in order to conserve Φ. Thus these particles will find themselves at a new radius and a new value of magnetic field strength. But conservation of the first adiabatic invariant $\frac{p^2 \sin^2 \alpha}{2m_o B}$ requires $\frac{p^2}{B}$ to remain constant, where p is the particle relativistic momentum [Northrop, 1963; and Coleman, 1961], m_o is the particle rest mass, and the pitch angle α of the charged particles is assumed to be 90°. Therefore, p^2 (and the kinetic energy) is changed as B changes. In summary, particles starting at $r = r_1$ with $B = B_1$ and momentum $p = p_1$ find themselves later at r_2 with field B_2 and momentum p_2. We rewrite B_o in terms of the vector potential $\vec{A}$; $\vec{B}_o = \nabla \times \vec{A}$. At the equator $\vec{A}(r) = \hat{a}_\varphi \frac{M}{r^2}$ where the earth's dipole magnetic moment is $M = -0.312$ gauss (earth radii)^3. Then by Stokes' theorem $\oint \nabla \times \vec{A} \cdot \vec{ds} = \oint \vec{A} \cdot \vec{dl} = \frac{M}{R} \int_0^{2\pi} d\varphi$ and the flux invariant is $\Phi(R) = -2\pi \frac{0.312}{R} + 2\pi \int_0^R \Delta B(r,t) r \, dr$, where R is in units of earth radii. In order to conserve Φ as B changes between times t_1 and t_2, we must have $\Phi(R,t_1) = \Phi(R,t_2)$, which yields

$$\frac{1}{R(t_1)} = \frac{1}{R(t_2)} - \frac{1}{0.312} \int_0^{R(t_2)} \Delta B(r,t_2) r \, dr + \frac{1}{0.312} \int_0^{R(t_1)} \Delta B(r,t_1) r \, dr. \quad (1)$$

This is the expression for the initial location $R(t_1)$ of particles which are found at $R(t_2)$ after the disturbance field has changed from $\Delta B(r,t_1)$ to $\Delta B(r,t_2)$. This equation is solved in a straight-forward manner if $\Delta B(r,t_1) = 0$, and by successive approximations if $\Delta B(r,t_1) \neq 0$. When the locations are thus determined from conservation of the flux invariant, the conservation of the first invariant leads to

$$\frac{p_2^2}{p_1^2} = \frac{B_2}{B_1} = \frac{B_o(R_2) + \Delta B(R_2,t_2)}{B_o(R_1) + \Delta B(R_1,t_1)} . \tag{2}$$

The directional differential intensity of particles with energy in the range dE at E is given by $j'(E) = p^2\tau$, and Liouville's theorem [Ray, 1959] assures us that the density in phase space, τ, is conserved along the particle trajectory. Thus

$$\frac{j'(E_2, R_2)}{j'(E_1, R_1)} = \frac{p_2^2}{p_1^2} , \tag{3}$$

where the kinetic energies E_1 and E_2 are connected by equation (2) and the relativistic relation between E and p. Thus we can follow these particular particles along their trajectory and can predict the intensity due to them at any point, but their energies are changing. We want to determine the energy spectrum in order to compare intensities of electrons of energies greater than the detector threshold E_t at the two locations. Assume a differential energy spectrum of the form $j'(E) \propto E^{-n}$, so that

$j'(E_1,R_1) = j'(E_t,R_1)\left(\frac{E_1}{E_t}\right)^{-n}$. Thus equation (3) with $E_2 = E_t$ yields

$$j'(E_t,R_2) = \frac{p_2^2}{p_1^2}\, j'(E_1,R_1) = j'(E_1,R_1)\left(\frac{E_t}{E_1}\right)^{n} \frac{p_2^2}{p_1^2} .$$

Substituting equation (2) and utilizing the relativistic expression $p^2 = m_o E(\gamma + 1)$, where E is the kinetic energy and p, m_o, and γ have their usual relativistic meanings, we obtain, after several algebraic manipulations

$$\frac{j'(E_t,R_2)}{j'(E_t,R_1)} = \left(\frac{B_2}{B_1}\right)^{n+1} \left[\frac{1 + \sqrt{1 + \bar{E}_t(2 + \bar{E}_t)\frac{B_1}{B_2}}}{2 + \bar{E}_t}\right]^{n} , \qquad (4)$$

where $\bar{E}_t$ is the threshold kinetic energy in rest mass units. This equation applies to the intensities at R_1 before the magnetic field change and at R_2 after the change. The term in square brackets is strictly a relativistic correction factor, and goes to unity for non-relativistic energies. For very high energies, this term (with exponent) goes to $\left(\frac{B_1}{B_2}\right)^{n-2}$. The effects of this correction are negligible for the 40 keV electrons and are less than about 20% for the 2 MeV electrons. If the energy spectrum is unchanged, which is true in the non-relativistic case, equation (4) also gives the ratio of the integral intensities. Coleman [1961] has shown that the spectrum index is changed, but only slightly for reasonable values of B_2/B_1, and such a change is ignored here.

The integral intensities and spectra were obtained from the observations on October 31, 1964, when $D_{ST}(H)$ was -9 gammas. Then for selected radial distances equation (1) was used to find the initial location, and the initial intensity at that point was used with equation (4) to predict the intensity at the selected location and time. Provisional values of $D_{ST}(H)$ were kindly computed by John Craven for the period of the observations. $D_{ST}(H)$ was used to scale the disturbance field $\Delta B(r,t)$ which was patterned after the deviations from the reference field as reported by Cahill [1966] for several passes of Explorer 26 during the time of the April 17, 1965 geomagnetic storm. The radial profile of the model $\Delta B(r,t)$ at several times during the storm of November 1, 1964, is shown in Figure 13. The $D_{ST}(H)$ hourly averages are shown in Figure 14, while the smooth model of $D_{ST}(H)$ shown in Figure 15 was used for the calculations. The October 31 observations determined the initial intensity distribution and predicted intensities were computed at 5 γ intervals of $D_{ST}(H)$ thereafter. Before comparing predictions with observations, we present the predictions for arbitrary $D_{ST}(H)$, as functions of $D_{ST}(H)$, in the next four figures. Figure 16 shows the computed locations (as functions of $D_{ST}(H)$) of particles which were on each L shell at the initial time (when $D_{ST}(H) = -9$). Note that the particles move outward at all L shells as $D_{ST}(H)$ decreases. These results are similar to those of Dessler and Karplus [1961] for $L \leq 5$. For larger values of L the present work has smaller values of ΔL. Figures 17, 18, and 19 show the ratios of the predicted intensities to the initial intensities as functions of $D_{ST}(H)$, for detectors A1, B2, and C. The calculations were performed according to equation (4) for the directional intensity of particles at the equator. However, it has been shown above that the observed pitch angle distributions of intensities at the equator are peaked at $\alpha_o = 90°$, but are relatively isotropic and relatively constant, indicating that the directional intensity of particles with $\alpha_o = 90°$ is approximately a constant fraction of the omnidirectional intensity. Furthermore, the effects of adiabatic motion are not expected to significantly alter the pitch angle distribution of equatorial intensities (see Krymov and Tverskoy [1964] on pitch angle changes). On this basis the predictions are applied to the measured omnidirectional electron intensities in the equatorial plane. Note that the intensities increase at L-values outside the peak of the outer zone, and decrease inside with increasing magnitude of $D_{ST}(H)$. This is due to the shape of the radial intensity profile and to the outward particle motion. There is a decreased intensity above the threshold due to betatron deceleration, but this is overpowered beyond the outer zone peak by the increase due to the steep radial intensity gradient. At distances just outside the "slot", the radial intensity gradient and betatron deceleration combine to produce even lower intensities, while just inside the "slot", the betatron deceleration overpowers the increase of intensity due to the radial intensity gradient, again producing a deeper "slot".

Figures 20 and 21 show the contours of constant electron intensity as measured with the detectors A1 and B2, respectively, predicted from the data of October 31 and the smoothed $D_{ST}(H)$ values shown in Figure 15. The times of the spacecraft passes through the outer zone are indicated by the arrows marking times of perigee. The contours are labelled with the detector counting rate. The predicted A1 and B2 intensity contours ($E > 40$ keV and $E > 130$ keV, respectively) change noticeably with $D_{ST}(H)$, moving outward in the outer zone, but moving inward in the region inside the minimum intensity near $L = 4$. Thus a well-defined decrease in intensity occurs in the region of the "slot" where the intensity was already at a minimum. Note the contours which develop near $L = 4$ during the depth of the main phase and persist for 1-1/2 to 2 days. There is also an enhancement of the intensities at the maximum of the outer zone. The predictions for detector C, shown in Figure 22, show only small intensity changes except at $L \sim 4$ and $L \sim 4.5$, where the contour just inside the maximum moves out in L by more than 0.5. Note that the contours of constant intensity of electrons ($E > 2$ MeV) as measured with detector C are all displaced outward for larger magnitudes of $D_{ST}(H)$. This feature is similar to the behavior of the predicted contours of constant intensity of electrons of energies above the thresholds of detectors A1 and B2, with contours outside the "slot" moving out and the others moving in, although the individual particles all move in the same direction, as indicated in Figure 16. For detector C the "slot" is close in and data are not presented for the region inside it. Since the longitudinal drift periods [Lew, 1961] of 40 keV and of 130 keV electrons at L = 4 are about 4 hours and about 1-1/2 hours, respectively, it is to be expected that these lower energy particles would not respond adiabatically to the fast initial depression indicated by $D_{ST}(H)$, but would respond adiabatically to the slower phases of the storm. The longitudinal drift period of electrons of energy 2 MeV at L = 4 is about ten minutes, so they should respond adiabatically to faster phases of the storm than the electrons of energies 40 keV or 130 keV.

The time resolution possible with the spacecraft orbit is not fine enough to allow a detailed check on the agreement of the predicted intensity contours with observed ones. The arrows in Figures 21, 21, and 22 show the times of perigee, thus indicating the temporal resolution possible with this spacecraft. A quantitative check on the counting rate predictions is provided by comparing the observed relative intensities with the predicted ones.

Values of the quantity R = (observed relative intensity/relative intensity predicted from calculations assuming adiabatic motion) near unity will indicate behavior consistent with adiabatic motions, while values far from unity will indicate that non-adiabatic processes are dominant. It is also possible that non-adiabatic losses and increases can combine to yield R ~ 1. The values of this parameter R are presented in Table II for all three detectors for four passes after the initial one on October 31, which was used as the base for the calculation of the ratios involved. The values of R tabulated for detectors A1 and B2 are always within a factor of three of unity, except on November 2, when R = 4.8 and 6.9 at L = 4 and 5, respectively, for detector A1, and R = 3.7 at L = 5 for detector B2. The most significant variations are seen in the detector C data, where R has the low values of 0.13, 0.14, and 0.20 at L = 5 on November 2 and 5, and the higher values of 5.6 to 9.4 at L = 7 on November 2, 5, and 7. Thus the electron (E > 2 MeV) intensities observed with detector C clearly exhibit violations of adiabatic motion during this period with intensities significantly higher than predicted at L ~ 7-8 and significantly lower than predicted at L ~ 5. The intensities of lower energy electrons measured by detectors

Table 2

Values of the parameter R = (observed relative counting rate/predicted relative counting rate)

Detector	L	Nov. 2 OUT	Nov. 5 IN	Nov. 5 OUT	Nov. 7 IN
	8	1.4	0.92	1.5	0.87
	7	1.3	1.1	1.3	0.78
A1	6	2.4	1.7	2.0	0.96
	5	6.9	2.2	1.9	1.1
	4	4.8	1.3	0.91	1.2
	3	1.2	1.2	1.2	0.39
	8	2.0	1.4	2.7	2.7
	7	1.0	1.1	1.2	1.1
B2	6	1.6	1.2	1.2	1.0
	5	3.7	1.2	1.2	0.94
	4	1.7	0.85	0.60	0.66
	3	0.35	0.42	0.44	0.96
	8	6.7	2.4	5.4	5.6
	7	7.2	5.6	7.6	9.4
C	6	0.30	0.28	0.34	0.58
	5	0.13	0.14	0.20	0.41
	4	0.37	0.70	0.81	0.64
	3	1.3	0.82	0.96	1.1

A1 ($E > 40$ keV) and B2 ($E > 130$ keV) clearly contradict the predictions on November 2, where the detector B2 measurement of intensity of 3.7 times the predicted intensity at $L = 5$ is high enough to be significant, and the detector A1 measurement of intensity ratios of 4.8 and 6.9 at $L = 4$ and 5 clearly indicates non-adiabatic motions.

Note that the intensities measured with both detectors A1 and B2 were higher than predicted at $L \sim 4$-5 on November 2, while the intensity measured with detector C at the same L was lower than predicted, which suggests that the non-adiabatic process (if there is only one) in operation here is quite energy-dependent or that the non-adiabatic processes dominating the intensities of the low energy ($E > 40$ keV) electrons are different from those controlling the intensities of the high energy ($E > 2$ MeV) electrons.

The effects of adiabatic motions as computed above for relatively small magnetic field variations, as well as the effects predicted for large magnetic disturbances, suggest that such motions may play a role in the formation of the persisting slot structure between the two intense belts of trapped particles. For example, for a large magnetic disturbance characterized by a $D_{ST}(H)$ decrease from 0 to -200γ, the intensities in the slot as seen by detector

C are predicted to decrease by about a factor of 6 while the slot moves out by 0.4 R_E. The intensities in the slot as seen by detector A1 are predicted to decrease by a factor of about 400 and the slot moves out by 1.3 R_E. The outer zone maximum seen by detector C decreases by 10 and moves out 2.5 R_E; the maximum seen by detector A1 decreases by a factor of 2 but moves out by 5 R_E. The inner zone peak, however, remains at nearly a constant location and decreases in intensity by only a factor of about 0.6, as seen by both detectors. Thus, the adiabatic predictions show that the inner zone region ($L < 2.5$) remains relatively stable (as might be expected since ΔB there is small compared to B_o), while the outer zone peak location and slot depth undergo large changes in response to large magnetic disturbances. The effects of the adiabatic motions are reversible, however, so non-adiabatic processes are necessary in order to obtain any net changes in the radiation zone structure or to obtain any net apparent sources or sinks of particles.

The rapid fluctuations at the beginning of a magnetic storm main phase constitute one possible source of non-adiabatic motion. To find the net effect of a storm on particle intensities, it is necessary to find the effects of the rapid magnetic fluctuations at its beginning, then follow the adiabatic motions (if adiabatic conditions apply) during its slower recovery, such as was done by Davis and Chang [1962], for example. If the initial phase results in an inward radial displacement (or none) or a small enough outward one, then the combination with the adiabatic inward motion during the recovery results in a net inward motion of particles for the period of the storm. The changes in individual particle energies and in intensities will depend on the details of the processes acting on the particles. As an example of the possible effects of adiabatic motion during only a part of the time, we consider the recovery phase of the model storm used herein. The peak intensity of 2 MeV electrons is predicted to move inward from $L \sim 4.75$ to $L \sim 4.5$, while $D_{ST}(H)$ recovers from -30γ to -10γ in about 4 days. This corresponds to an inward velocity of the peak of about 0.06 L/day K which may be compared with the velocity of about 0.1 L/day at this L reported by Craven [1966]. The velocity of about 0.4 L/day reported by Frank [1965] describes the motion of the inner edge of a moving peak at this L. The events reported by Frank and by Craven occurred during periods of relative magnetic quiet following disturbances. A look at $\dot{D}_{ST}(H)$ for these periods shows a generally rising value of $D_{ST}(H)$ (or slow recovery) for certain periods while for others there is little average change. For all there are numerous short-term variations. The L-dependence of the velocity of the inward motion computed here is much less than that observed in the two investigations above, the apparent velocity at $L \sim 6.2$ calculated here being about twice that at $L \sim 5$, whereas Craven exhibits velocities at $L \sim 6.2$ which are about 25 times those at $L \sim 5$. Thus the adiabatic mechanism investigated here produces inward radial motion qualitatively similar to that which has been observed by Frank et al. [1964], Frank [1965], and Craven [1966], but quantitatively the computed inward velocities are not in agreement with the observations. The computations of inward velocity are applicable only during the slow recovery phase of a magnetic storm. In addition, this mechanism cannot, by itself, repopulate the outer zone after its depletion, but rather can only cause the outer zone peak to move radially and increase slightly in intensity.

V. DISCUSSION AND CONCLUSION

The pitch angle distributions of intensities of outer zone electrons ($E > 40$ keV, > 130 keV, and > 2 MeV) near the magnetic equatorial plane have previously been reported for selected periods of time. Farley and Sanders [1962] presented equatorial angular distributions of intensities of electrons ($E > 200$ keV) at 21,000 km radial distance, derived from omnidirectional intensity measurements obtained with Explorer 6 in 1959. Their report showed approximately isotropic intensity distributions at the equator, except for an apparent low intensity near pitch angles $\alpha = 90°$ and in the loss cone near $\alpha = 0°$. The results differed from those reported by Fan et al. [1961] for electrons ($E > 13$ MeV) at the same radial distance, primarily because of the different definition of angular distribution employed by Fan et al. The latter, however, showed that the omnidirectional intensity could be approximated by $I = I_o\ (B/B_o)^{-x}$, where I is the intensity, B is the magnetic field, and the subscript zero indicates values at the magnetic equator. This is the dependence expected if the directional intensity at the equator is given by $j(\alpha) \propto \sin^{2x}\alpha$ (see Section III). In fact, Fan et al. used $\sin^{2x}\alpha$ in the definition of their averaged angular distribution. The data presented in their Figure 3 indicate $x \sim 0.56$. Hence their data are consistent with a directional electron ($E > 13$ MeV) intensity distribution $j(\alpha) \propto \sin^{1.1}\alpha$, which is in good agreement with the present results for lower energies. Hoffman et al. [1962] presented distributions also derived from omnidirectional intensities. Their intensities of electrons ($E \gtrsim 1$ MeV) were approximately isotropic for pitch angles $\alpha \gtrsim 40°$ at 17,000 km and 22,400 km, but at 28,000 km the intensity at $\alpha = 60°$ was only 1/5 the intensity at $\alpha = 90°$. Serlemitsos [1966] reported local pitch angle distributions of intensities of electrons ($E \gtrsim 100$ keV) obtained with Explorer 14. The relative isotropy of the intensities at $L \sim 4$-8 was stressed, and the observation of distributions of intensity peaked parallel to the field at distances beyond $\sim 8\ R_E$ was reported. The latter result has been confirmed at 8-14 R_E by detectors borne on OGO 1 [Hills, 1967]. In the present research the angular distributions of intensities of electrons ($E > 40$ keV and $E > 130$ keV) were approximated by $\sin^n\alpha$ for all the data obtained throughout the period September-December, 1964. The values of n determined at $L \sim 4$-8 were consistently $\lesssim 1$ for both energy ranges. The relative isotropy is a persisting feature of energetic electron intensities in the outer zone (L ~ 4-8) near the magnetic equatorial plane. Note that such a low value of n indicates relative isotropy even if the pitch angle distribution is not accurately given by the function $\sin^n \alpha$, since n is determined from the observed spin modulation of the detector counting rates. However, a sharply decreased intensity over a range of α of a few degrees will just be averaged out by the wide-angle detectors used here. Hence, no information is obtained with regard to the intensity in the loss cone $\alpha_o \lesssim 5°$ (or in a small range near any angle α) except in the sense of an average over the detector field of view. Pfitzer et al. [1966] have reported the angular distributions of intensity and the differential energy spectra for electrons (E = 50 keV - 4 MeV) for selected times in 1964, also obtained with detectors on OGO 1. For $\alpha \gtrsim 45°$ the relative isotropy is apparent and is in agreement with the present observations.

The 2-point integral power law energy spectrum indices were determined for all the data obtained throughout the period September-December, 1964, from the omnidirectional intensities of electrons (E > 40 keV, > 130 keV, > 2 MeV). The median value of the spectrum index derived from the intensities of electrons of energies E > 40 keV and E > 130 keV increased from ~ 1 at L = 5 to ~ 2.1 at L = 9. For the electrons of energies E > 130 keV and > 2 MeV the median index increased from ~ 3 at L = 5 to ~ 4 at L = 9. These results are consistent with the more detailed differential electron energy spectra (E = 50 keV - 4 MeV) presented by Pfitzer et al. [1966] for selected times in late 1964. The intensities of energetic electrons in the outer zone have been presented above. In general, the outer zone intensities of electrons (E > 40 keV, > 130 keV, and > 2 MeV) reported herein for the period September-December 1964, are consistent with those reported for periods of time three years earlier and later. The temporal variations at low latitudes of electron intensities observed with OGO 1 near solar minimum were as large as those observed in 1961 (nearer to solar maximum) with Explorer 12 [Rosser et al., 1962]. The character of the temporal intensity variations has been noted by many investigators. Correlations of intensities with many factors have been reported, including the occurrence of magnetic storms, $D_{ST}(H)$, ring currents, K_p, and solar effects. McIlwain [1966b] has suggested a classification of effects causing temporal variations and has demonstrated some success in sorting out the various effects by separating a steady exponential intensity decay in time from intensity changes well correlated with magnetic field fluctuations.

The omnidirectional electron intensities reported herein at the magnetic equator near the end of October, 1964, may be taken as typical of the period September-December 1964. At L = 5 these intensities were $\sim 2 \times 10^7$, $\sim 8 \times 10^6$, and $\sim 2 \times 10^4$ cm^{-2} sec^{-1} for electrons of energies $E > 40$ keV, > 130 keV, and > 2 MeV, respectively. At L = 3 the intensities of electrons in the same energy ranges were $\sim 2 \times 10^7$, 1.5×10^6, and $\sim 8 \times 10^2$ cm^{-2} sec^{-1}, respectively. In addition, there were large temporal variations of these intensities. At L = 5 the intensities varied by factors of ~ 100, ~ 50, and ~ 650 for electrons of energies $E > 40$ keV, > 130 keV, and > 2 MeV, respectively. On a long term basis (years), intensities of electrons as reported here have been relatively steady, showing no radical change from solar maximum to solar minimum. The relatively low intensities near the equatorial plane reported herein at the end of 1964 should be considered as primarily a short-term fluctuation, similar to those seen at other times, e.g., in mid-December 1962 [Frank et al., 1964]. The outer zone intensities are evidently near a dynamic equilibrium which is relatively unaffected by the solar activity cycle, although the solar activity does affect the spatial structure of the trapping region [Frank and Van Allen, 1966]. This fact lends support to the existence of an intensity-limiting mechanism independent of the solar cycle such as the one reported by Kennel and Petschek [1966].

The calculations presented here are applicable to the motion of a charged particle mirroring in the magnetic equatorial plane during a particular slow perturbation of the earth's magnetic field. The meaning of "slow" depends on the longitudinal drift velocity of the trapped particles under investigation. The adiabatic theory is applicable if the longitudinal drift period of the particle is short compared to the time required for a substantial magnetic field change. Then the effects of the magnetic field perturbations on the particle intensities will be as calculated herein. A similar calculation at low L-values ($L = 3.6$ and 3.8) using a spatially uniform perturbation of the magnetic field has been recently reported by McIlwain [1966b] for intensities of electrons ($E > 0.5$ MeV). The adiabatic approach used here avoids the complications of following the particle along its trajectory as it gyrates around the magnetic field line, drifts longitudinally, and reacts (by the $\vec{E} \times \vec{B}$ radial drift) to the electric field induced by the magnetic field fluctuation. The effect of the magnetic field fluctuations can be viewed as an acceleration due to the drift of the particle parallel to the induced electric field plus the betatron acceleration acting on the particle as it gyrates about its guiding center. Use of the adiabatic approach also eliminates the separate handling of these two acceleration processes.

Extension of these calculations to particles with pitch angles $\alpha_o \neq 90°$ would result in much more complicated calculations, but the results would not be expected to differ drastically from those of the present case. The guiding centers of particles with $\alpha_o \neq 90°$ will oscillate in latitude, following the lines of force of the total field (dipole plus perturbation) rather than the dipole field lines. When particles having pitch angles $\alpha_o \neq 90°$ are considered the conserved magnetic moment is $\mu = \frac{p^2 \sin^2 \alpha}{2 m_o B}$ and changes in α can be produced as well as changes in p^2 (i.e., in energy) by the fluctuations of the magnetic field. For values of α_o close to 90° the present calculation (which assumes $\alpha_o = 90$,) is expected to serve as an approximation to the exact solution. For such particles (mirroring near the equatorial plane), the pitch angle changes will be small [Krymov and Tverskoy, 1964]. The latitudinal oscillations will take place along the field lines, hence the flux invariant calculated for a location in the equatorial plane will also be correct for these particles. This indicates that the calculations made for particles mirroring at the equator can be approximately applied to other particles as well.

The predicted relation between intensity of electrons ($E > 2$ MeV) and $D_{ST}(H)$ is shown in Figure 19 and can be approximated by $I \propto \exp \frac{D_{ST}(H)}{K}$ for $L \lesssim 4$. A value of $K = 110\ \gamma$ provides a fit good to within 4% for $0 \geq D_{ST}(H) \geq -80\ \gamma$ at $L = 3$. The fit with $K = 52\ \gamma$ at $L = 4$ is good to within $\sim$ 1% for $D_{ST}(H) \geq -60\ \gamma$, and is about 15% off at $-80\ \gamma$. An exponential dependence was also predicted by McIlwain [1966b] at $L = 3.6$ and $L = 3.8$ and was observed for intensities of electrons ($E > 0.5$ MeV). McIlwain calculated the values $K \sim 40 - 90\ \gamma$ and found that $K = 54\ \gamma$ fit the observations well, after correction for an exponential decay in time. Forbush et al. [1962], with a 302 GM tube on Explorer 7, found a similar correlation between the counting rate and the ring current field measure U. Their data indicates $K \sim 33\ \gamma$ at

$L = 4.1$ for electrons ($E > 1.1$ MeV). Thus the present results are in agreement with other calculations made at low L-values as well as with other observations. However, the data of Forbush et al. indicated a negative value of K for $L < 3.4$. This disagrees with the present predictions, which indicate that K is positive for $L \lesssim 4$ and negative for $L \gtrsim 6$. McIlwain [1966a] reported the predictable changes in intensity of protons ($E > 40$ MeV) at $L < 2.4$, and Davis and Williamson [1966] reported variations of intensities of protons ($E > 140$ keV) which could be described by the exponential dependence used above with $K \sim 120\ \gamma$. But Davis and Williamson also showed that for electrons ($E = 20 - 100$ keV) the intensity variations indicated $K \sim -25\ \gamma$ at $L = 3.75$. The explanation of the apparently conflicting observations of the correlation of electron intensities with $D_{ST}(H)$ is not known. McIlwain [1966b] suggests that the currents at the magnetospheric boundary, which contribute to $D_{ST}(H)$, and the asymmetry of the magnetic storms may be factors.

It is clear that large particle intensity changes observed in the outer zone are correlated with magnetic field fluctuations, and the calculations reported here show that adiabatic motions of charged particles can produce significant intensity changes through the combined effects of radial motion and acceleration by betatron effects during magnetic storms. The reported observations of electron intensities with OGO 1 are compared with the predictions and show that at $L \gtrsim 4$ large non-adiabatic effects were observed. At $L \lesssim 3$ both observed and predicted intensity changes were small. Inward radial motion of intensity peaks during the slow recovery phase of magnetic storms is predicted by the theory of adiabatic motions, but the apparent velocity obtained is not in agreement with the observations of Frank [1965] or of Craven [1966], the predicted velocity being less dependent on L than the observed velocity.

The calculations performed in this research utilize a model of the equatorial plane magnetic field disturbance which is patterned after the observations of Cahill [1966]. The prediction of energetic electron intensity variations due to adiabatic motion during magnetic storms is extended to the range $L \sim 3$-9. Outer zone energetic electron intensities are predicted to decrease at $L \lesssim 5$ with moderate ($\lesssim 80\ \gamma$) decreases of $D_{ST}(H)$ and to increase at $L \gtrsim 5$. Qualitatively similar results are found for large magnetic storms (~ 150-$200\ \gamma$ decrease), with intensity variations which decrease the outer zone peak intensities, greatly accentuate the low intensities in the slot, and move both the outer zone peak and the slot to larger radial distances. There is a negligible effect on the location of the inner zone peak and only a small effect on the intensities near the peak. This behavior suggests that the location of the slot may be due to the steep spatial gradient (near L = 4 in this model) of the magnetic field disturbance which appears in the magnetosphere during the magnetic storms. This field perturbation presumably controls at least some of the loss mechanisms which produce the slot, just as it controls the adiabatic motions investigated herein.

APPENDIX I

Detector Energy Thresholds

The counting efficiency of a GM tube is proportional to the transmission of the detector window (or wall) for the particle and energy in question if the contribution to the counting rate due to bremsstrahlung from non-penetrating particles is negligible, as will be the case for spectra which are not too steep. For electrons the transmission of the window as a function of energy is not a step function, but rather varies smoothly with energy (see Figure 1 of Craven [1966], for example). The transmission of the window of the unshielded type 6213 GM tubes can be measured by use of a mono-energetic electron gun beam to find the ratio of the counting rate to incident electron intensity as a function of electron energy.

A Po^{210} alpha particle source was used to measure the air equivalent thicknesses of the mica windows of the OGO 1 detectors. This measurement confirms that the window thicknesses of the present detectors are similar to those of several detectors which have been subjected to electron gun calibrations in this laboratory.

Energy thresholds of these detectors for protons are well-defined and can be obtained from tables, but for electrons we must take into account the function f(E), which is the measured detection efficiency of the detector for incident electrons of energy E. The spectrum of the incident electrons must be considered along with f(E) in order to arrive at an effective threshold energy for the detector. Consider an effective threshold energy E_c to be defined as the threshold of an idealized detector ($f(E) = 1$ if $E \geq E_c$, $f(E) = 0$ otherwise) which has the same counting rate as the real detector. That is, for an incident differential energy spectrum $j'(E)$, we have the counting rates

$$R_{ideal} = \int_{E_c}^{\infty} j'(E)dE = \int_{0}^{\infty} j'(E)\ f(E)dE = R_{actual}.$$

The integrals must be evaluated only over the energy range $E < E_1$ where f(E) is not unity, since the integrals over higher energies cancel each other when the equation is rewritten as

$$\int_{E_c}^{E_1} j'(E)dE + \int_{E_1}^{\infty} j'(E)dE = \int_{0}^{E_1} j'(E)\ f(E)dE + \int_{E_1}^{\infty} j'(E)dE.$$

If now $j'(E) \propto E^{-\gamma-1}$, evaluation of the integral on the left yields

$$\frac{E_c^{-\gamma} - E_1^{-\gamma}}{\gamma} = \int_0^{E_1} j'(E)\, f(E)dE. \quad \text{Hence, } E_c = [E_1^{-\gamma} + \gamma \int_0^{E_1} E^{-\gamma-1} f(E)dE]^{-1/\gamma}.$$

This has been evaluated with a computer, using f(E) typical of several unshielded type 6213 detectors, with the result that E_c is relatively insensitive to γ in the range $\gamma = 0$ to 10, ranging from 44 keV at $\gamma = 0$ to 37 keV at $\gamma = 10$. Thus, 40 keV is taken as the energy threshold of the type A detectors for detecting electrons.

For the C detector, higher energies are needed than are available with the laboratory electron gun. A beta-ray spectrometer was used to obtain the relative detection efficiency for electrons of energy up to about 1.6 MeV. This response, which rises rapidly between 1 and 1.5 MeV, is similar in form to previously determined responses of similarly (not identically) shielded detectors. On the basis of the measured response and the range-energy relations for electrons we take 2 MeV as the nominal threshold energy for detecting electrons with detector C. For an incident differential energy spectrum of the form E^{-n}, the factor $\frac{1}{\epsilon G_o}$ is about 10, to within a factor of 2 for n in the range 2-5.

The type B detectors are shielded by 10.2 mg/cm^2 of aluminum in addition to the mica window. Thus we take 130 keV as the nominal threshold energy for detection of electrons with the type B detectors.

The geometric factors of the directional detectors are discussed in Appendix II and a table of geometric factors and shielding for the electron and proton detectors is included in the Description of the Apparatus.

APPENDIX II

Geometric Factors and Effects of an Anisotropic Angular Distribution of Charged Particle Intensities

The directional GM detectors used in this work have conical fields of view with a half-angle of 45°, and the relative response of the detector to particles incident at an angle θ from the center of the field of view depends on θ. For an idealized case the response is expected to be proportional to $\cos \theta$, since this represents the dependence of the area of the projection of the window in the direction θ. However, in the case of the detectors used for these observations the relative response $f(\theta)$ is approximately given by $\cos^5 \theta$, for example, for detector A1.

The relative response was measured with the collimated beam from a radioactive $T\ell^{204}$ beta particle source in an evacuated chamber. The detector could be rotated about a vertical axis lying in the plane of the detector window. The source holder could be rotated about a horizontal axis also lying in the plane of the detector window. The center of the detector window was carefully located at the intersection of these two axes and the electron beam from the beta source was centered on this intersection (i.e., centered on the detector window). With this apparatus the detector counting rate was measured as a function of θ in two perpendicular planes normal to the mica window. The counting rate responses in the two planes were found to be similar, so they were used to represent the average relative response function $f(\theta)$ as a function of θ only, with $f(\theta)$ normalized to unity at $\theta = 0°$.

With the fraction of all incident particles penetrating the window denoted by ε, the detector counting rate R due to an incident directional flux of intensity j is given by $R = A\varepsilon \int_{\Omega} j\ f(\theta) d\Omega$, where A is the area of the collimator aperture, Ω is the solid angle viewed by the detector, and $f(\theta)$ is the normalized response function described above. For computational convenience assume a pitch angle distribution $j = j_{\perp} \sin^{n}\alpha$, where α is the angle to the magnetic field vector. Let the solid angle Ω be described by the integration variables θ, the angle from the center of the field of view, and φ, the azimuthal angle around the $\theta = 0°$ axis. Then the above expression becomes

$$R = A\varepsilon j_{\perp} \int_{0}^{2\pi} d\varphi \int_{0}^{\theta_c} d\theta\ f(\theta) \sin\theta \sin^{n}\alpha, \qquad (1)$$

where θ_c is the half angle beyond which $f(\theta)$ becomes zero. Before integration, $\sin^n\alpha$ must be rewritten in terms of the integration variables θ and φ and of the pitch angle distribution parameter n. This is done by two applications of the spherical harmonic addition theorem to the geometry of the problem.

For a diagram illustrating the first application refer to Figure 23a, where $\overrightarrow{\mathrm{DET}}$ is the direction of the center of the detector (i.e., $\theta = 0°$) and δ is the fixed angle (about 55°, but slightly different for the three different detector directions) between the spin vector and $\overrightarrow{\mathrm{DET}}$. The rotation angle about the spin vector is ψ, with $\psi = 0°$ when the spin vector, $\vec{B}$ vector, and detector direction are coplanar. For the figure, and the theorem mentioned above,

$$\cos\beta = \cos\delta \cos\Gamma + \sin\delta \sin\Gamma \cos\psi. \tag{2}$$

For the second application of the theorem see part b of Figure 23, where the integration variable θ ranges from 0° to θ_c while the azimuthal coordinate φ goes from 0 to 2π. Hence

$$\cos\alpha = \cos\beta \cos\theta + \sin\beta \sin\theta \cos\varphi. \tag{3}$$

Now write $\sin^n\alpha = (1 - \cos^2\alpha)^{n/2}$, substitute (3) into (1), and obtain

$$R_{calc} \equiv \frac{R}{\epsilon J_o} = \frac{Aj_\perp}{J_o} \int_0^{2\pi} d\varphi \int_0^{\theta_c} d\theta\, f(\theta) \sin\theta \Big\{1 - \cos^2\beta \cos^2\theta$$

$$-2\cos\beta \sin\beta \cos\theta \sin\theta \cos\varphi - \sin^2\beta \sin^2\theta \cos^2\varphi\Big\}^{n/2} . \qquad (4)$$

β is the angle between $\vec{B}$ and the detector and is not given directly, so equation (2) must be utilized in order to compute (4) from the known quantities δ, Γ, and ψ. R_{calc} is the calculated counting rate normalized to unit omnidirectional intensity J_o. Hence with R representing the observed detector counting rate (both R and R_{calc} depend on time and Γ), the omnidirectional intensity is

$$J_o = \frac{R}{\epsilon R_{calc}} . \qquad (5)$$

For the $\sin^n\alpha$ angular distribution used here $J_o = 2\pi \int_0^\pi j_\perp \sin^{n+1}\alpha\, d\alpha$, or

$$\frac{j_\perp}{J_o} = \frac{1}{4\pi \int_0^{\pi/2} \sin^{n+1}\alpha\, d\alpha} . \qquad (6)$$

The integral (6) is a standard one and is easily evaluated for positive integer values of n. The double integral in (4), however, must be performed numerically with a computer (for even or zero n and $f(\theta)$ in simple form the integral can be done analytically, but for $n > 4$ it rapidly becomes very long and tedious). With $\frac{j_\perp}{J_o}$ given by equation (6), the expression (4) was evaluated numerically on the U of I IBM 7044 computer for each of the six directional GM detectors, for a large number of combinations of the parameters ψ, n, and Γ. The result is a lengthy table giving the counting rate expected from each of the detectors during the spin cycle, under the assumption that the angular distribution of intensity is given by $j = j_\perp \sin^n\alpha$ with $j_\perp$ adjusted to provide unit omnidirectional intensity. In addition to the counting rates of the individual detectors, the sum of the rates of the three A detectors and the sum of the rates of the three B detectors are calculated, all these being calculated for each 10° interval of the spin rotation angle ψ from 0° to 360°. Also given is the modulation (defined as the ratio of the maximum rate in the spin cycle to the minimum rate in the spin cycle) for each detector. The preceding quantities are tabled for each 5° interval of Γ from 0° to 90°, and for integer values of n from 0 to 30.

For $n = 0$ the modulation is unity, but for non-zero values of n the modulation increases as n increases, depending also on the angle Γ between the spin vector and the magnetic field. This dependence of the modulation on n and Γ is shown in Figure 24, which is for detector A1 only, but which can be considered as typical of the general character of the modulation of all six GM tubes. If Γ is known and is not less than ~15° this figure (or, rather, a tabularized version of it) can be used to find the value of n appropriate to the observed modulation of the counting rate. The validity of this $\sin^n\alpha$ characterization of the pitch angle distribution is shown later, but it is clear from the figure that if $\Gamma \lesssim 15°$, the value of n is only poorly determined, since n varies rapidly with modulation for small values of Γ. The maximum values of modulation occur for $\Gamma = 55°$ because with the detectors at 55° to the spin vector this value of Γ is the only one which allows the detector to be aligned with the local magnetic field vector $\vec{B}$. This is illustrated in Figure 25a, where the solid bars denote the ranges in α covered during the spin cycle by the center of the detector for specified values of Γ. The dotted outline shows that for $\Gamma = 55°$ the value of α ranges from 0° to 110° so that, at different times in the spin cycle, the detector looks both at the weakest intensity (assumed parallel to $\vec{B}$) and at the strongest intensity (assumed perpendicular to $\vec{B}$). The same figure also shows that, for $\Gamma < 35°$, the center of the detector field of view never reaches a direction perpendicular to $\vec{B}$, while for $\Gamma = 35°$, the perpendicular point is just reached, so that the counting rate has only a single maximum during the spin cycle, corresponding to the closest approach to the plane perpendicular to $\vec{B}$. A diagram of such a case is given in Figure 25c, where $j(\alpha) = \sin^2\alpha$ has been drawn as an illustration of a pitch angle distribution. For Γ somewhat greater than 35° (depicted in Figure 25b) the detector starts at an angle α near 20°, passes through the plane perpendicular to $\vec{B}$, goes slightly away from it, and then passes through it again and returns to its initial azimuthal position. Thus the counting rate during a spin cycle exhibits two maxima separated by a shallow relative minimum, rather than a single maximum. As Γ increases, these two maxima move farther apart and the shallow minimum deepens, until Γ reaches 90°, where the counting rate exhibits two maxima (of equal height), and two minima (of equal depth) separated uniformly in time during a spin cycle. There are several observations of maxima of unequal height, indicating that $\sin^n\alpha$ does not even roughly approximate the pitch angle distribution in these cases, but these observations are at L-values of greater than about 8, and are not discussed in this paper. The time separating the maxima in a spin cycle (see Figure 26) is a function of the angle Γ only, so Figure 26 can be used to determine Γ approximately for comparison with the value of Γ determined from the Jensen and Cain 48 coefficient expansion for the geomagnetic field. For cases where the expansion field is expected to be valid, these two values of Γ are in reasonable agreement.

If the angular distribution is indeed approximately given by $\sin^n\alpha$, then the omnidirectional intensity J_o is related to R_{max}, the maximum observed counting rate in a spin cycle, by $J_o = \frac{R_{max}}{\epsilon R_{mcalc}}$, as shown by equation (5) above. Here R_{mcalc} is the expected maximum counting rate for the case of unit omnidirectional intensity, calculated according to equation (4). In other words, the omnidirectional geometric factor (for use with the maximum counting rate in a cycle) is $G_{mo} = R_{mcalc}$. The omnidirectional function $\frac{1}{G_{mo}}$ and the directional function $\frac{1}{g_m}$ (see below) are shown for detectors A1 and B2 in Figures 27 and 28, respectively, as functions of n for three different values of Γ. It is seen that for small Γ the results are less reliable than for high values of Γ, since $\frac{1}{G_{mo}}$ and $\frac{1}{g_m}$ both vary rapidly with n for $\Gamma \lesssim 15°$. The directional geometric factors g_m are calculated in a manner similar to the omnidirectional factors, and relate the observed maximum counting rate R_{max} to the directional intensity j_m of particles travelling in the direction of the center of the detector field of view at the instant of observation of R_{max}. Thus, $j_m = \frac{R_{max}}{\epsilon g_m}$. For the curve labelled $\Gamma \geq 35°$, the direction of view when R_{max} is observed is perpendicular to $\vec{B}$, while it is at an angle of 70° to $\vec{B}$ for $\Gamma = 15°$ and at an angle of 55° to $\vec{B}$ for $\Gamma = 0°$. The calculations are for an assumed $\sin^n\alpha$ angular distribution just as before, in which case the relationship of the omnidirectional factors to the directional factors is found by noting that $J_o = j_\perp 2\pi \int_0^\pi \sin^{n+1}\alpha \, d\alpha$ and $J_o = \frac{R_{max}}{\epsilon G_{mo}}$, so

$$j_m = j_\perp \sin^n\alpha = \frac{R_{max}}{\epsilon G_{mo}} \frac{\sin^n\alpha}{4\pi \int_0^{\pi/2} \sin^{n+1}\alpha \, d\alpha} . \qquad (6)$$

But $j_m = \frac{R_{max}}{\epsilon g_m}$, so g_m is defined in terms of G_{mo} and vice versa.

Thus, the omnidirectional intensity is obtained by multiplying the maximum directional intensity observed in a spin cycle by a factor depending upon Γ and n. For $n = 0$ the factor is 4π for all Γ, while for $n = 1$ it is 10.5 if $\Gamma = 15°$ and 9.9 if $\Gamma \geq 35°$.

The directional geometric factors must be computed as described above, but there is a more accurate way to obtain the omnidirectional intensity than to use the previously described function G_{mo}, which utilizes only the maximum and minimum counting rates during a spin cycle for its determination and which depends strongly on Γ and n. The better method is to utilize the instantaneous sum of the counting rates of the three mutually orthogonal detectors. This sum is expected to be fairly constant during one spin cycle since these three detectors cover such a large total solid angle. In detail, confirmation is obtained by carrying out the summation on the previously calculated expected counting rates, at all values of Γ and for reasonable n values. The sum remains nearly constant for all times in the cycle, even though the individual detector counting rates vary greatly. For example, when $n = 1$ and $\Gamma = 55°$ the maximum sum of the three detector counting rates in the spin cycle was only 7% greater than the minimum sum, whereas the maximum counting rate of detector A1 was 2.1 times the minimum counting rate during the cycle. Figure 29 shows the counting rate of detector A1 and the sum of the counting rates of all three detectors (taking into account the different geometric factors) and demonstrates the relative constancy of this sum compared to the individual rates. The solid lines drawn in the figure are calculated rates for the given values of n. No arbitrary shifting of axes was performed in order to produce agreement. The average over the two spin periods of the observed instantaneous sums was normalized to the average calculated rate of A1 for the two values of n used.

If a similar set of hypothetical detectors is studied, with normalized response functions as defined at the beginning of this section given by $f(\theta) = \cos\theta$, then for $n = 0$ (trivial case) and $n = 2$ the instantaneous sum is exactly constant over a spin cycle, regardless of orientation, although the constant can change slightly with the orientation. For other values of n there is a modulation of the sum at three times the spin frequency but with amplitude greatly reduced in comparison to the modulation of the individual counting rates, just as in the case of the actual detectors described above.

We may now take the average of the instantaneous sum of the A detectors as proportional to the omnidirectional intensity J_o, with the proportionality constant to be obtained from the calculated data at the pertinent values of n and Γ. But, since all of the detectors follow the same path during a spin cycle, we may look just at one of them, and find its average counting rate over several spin cycles. This will be 1/3 of the average of the instantaneous sums of the counting rates of the three mutually orthogonal detectors, so that we find the omnidirectional geometric factor appropriate to the average rate of a detector to be $G_o = \frac{S(n,\Gamma)}{3}$, where $S(n,\Gamma)$ is the calculated instantaneous sum of the counting rates of the three detectors for given n and Γ. However, S is relatively insensitive to n and Γ, deviating from its value for $n = 0$ by less than 2% when $n \leq 6$ for all values of Γ. When $n = 10$ the deviation is less than 7% for all Γ. Therefore, we take $\frac{1}{G_o} = 4.28 \times 10^3$ for detector A1 and 5.97×10^2 for detector B2, which are the values for $n = 0$, but which are adequate for a reasonably wide range of values of n as deomonstrated above.

APPENDIX III

Dead-time Corrections for the GM Tube Responses and Temperature Effects

After each signal pulse due to an ionizing event in a GM tube, there is a finite "dead-time" of around 50 to 100 μsec during which no pulse can be produced which is large enough to be detected, even if a particle does penetrate the active volume. At low counting rates this has negligible effect, but at high counting rates (of the order of 1/dead-time) a significant fraction of incident penetrating particles is not counted. Each detector, together with its associated circuitry, was calibrated in order to determine the relationship between the observed counting rate r and the rate R which would be produced if the detector had zero dead-time. This was done using a dc x-ray machine as a convenient point source of x-rays, measuring the response of the detectors as a function of distance from the source. The response satisfied the inverse square law at low counting rates, as expected, and the low rate data (plus the inverse square law) was used as a basis for determining the r vs R response at the higher counting rates obtained at closer distances. The r vs R response curve is extended to large R by suitable overlapping of the counting rate ranges used. As an illustration, for detector A1 the value of r is 890 counts sec^{-1} when R = 10^{3} counts sec^{-1}, 5.1 x 10^{3} counts sec^{-1} when R = 10^{4} counts sec^{-1}, and 1.45 x 10^{4} counts sec^{-1} when R = 10^{5} counts sec^{-1}. With detector C, r is 950 counts sec^{-1} when R = 10^{3} counts sec^{-1}, 4.9 x 10^{3} counts sec^{-1} when R = 10^{4} counts sec^{-1}, and reaches a maximum of 8.3 x 10^{3} counts sec^{-1} when R = 7 x 10^{4} counts sec^{-1}, declining at higher R to about 1.1 x 10^{3} counts sec^{-1} when R = 10^{6} counts sec^{-1}. These calibrations are good to about 10% for values of R up to 10^{4} counts sec^{-1} typically.

Selected parts of the calibrations described above were carried out at -20° C and +50°C, as well as at room temperature, to check for possible effects of temperature on the r vs R corrections. Such effects were negligible for the portions of the r vs R response curves which were needed for the observed counting rates used in the present investigation.

The University of Iowa experiment package contained a thermostat-controlled internal heater which was activated when the internal temperature dropped below about 4°C, and turned off at about 16°C. The upper limit of the package temperature was passively controlled by an appropriate coating of silicon monoxide on the outside of the spherical shell. The temperature of the package was included in the telemetered data. The external temperature rose rapidly from a minimum of about -7°C recorded soon after launch to about 18° on September 13, increased to 40° on October 12, then rose slowly to 50° on November 26. On December 2 the temperature was down to 40° due to the fact that the experiment power had been turned off, but rose again to about 48° when power was restored, then declined to about 35°C on December 31, 1964. At no time did the indicated temperature go above 50°C or below -7°C during the period September-December, 1964 covered here. The internal temperature sensor indicated a temperature of 35°C on September 13, rising slowly to 45° on October 12, to 49° on November 11, and to 50°C on December 18. Thus the temperature varied only slowly, and did not go above about 50°C or below about -7°, so corrections to the counting rates due to temperature dependence of the detectors are not necessary.

REFERENCES

Alfvén, H., Cosmical Electrodynamics, (Oxford, Clarendon Press, 1950).

Armstrong, T., "Morphology of the outer zone electron distribution at low altitudes from January through July and September 1963 from Injun 3", J. Geophys. Res. 70, 2077-2110 (1965).

Binsack, J. H., and Vytenis Vasyliunas, "Simultaneous shock compressions observed by the M.I.T. plasma experiments on IMP 2 and OGO 1," Trans. Am. Geophys. Union 48, 176 (Abstract), (1967).

Brown, W. L., and C. S. Roberts, "Observations of outer zone electrons on April 18, 1965, by the Explorer 26 satellite," Trans. Am. Geophys. Union 47, 135 (Abstract), (1966).

Cahill, Laurence J., Jr., "Inflation of the inner magnetosphere during a magnetic storm," J. Geophys. Res. 71, 4505-4519 (1966).

Coleman, Paul J., Jr., "The effects of betatron accelerations upon the intensity and energy spectrum of magnetically trapped particles," J. Geophys. Res. 66, 1351-1361 (1961).

Craven, John D., "Temporal variations of electron intensities at low altitudes in the outer radiation zone as observed with satellite Injun 3," J. Geophys. Res. 71, 5643-5664 (1966).

Davis, Leverett, Jr., and David B. Chang, "On the effect of geomagnetic fluctuations on trapped particles," J. Geophys. Res. 67, 2169-2179 (1962).

Davis, L. R., and J. M. Williamson, "Outer zone protons" in Radiation Trapped in the Earth's Magnetic Field, ed. McCormac (D. Reidel Publishing Co., Dordrecht, Holland, 1966), pp. 215-230.

Dessler, A. J., and Robert Karplus, "Some effects of diamagnetic ring currents on Van Allen radiation," J. Geophys. Res. 66, 2289-2295 (1961).

Fan, C. Y., P. Meyer, and J. A. Simpson, "Dynamics and structure of the outer radiation belt," J. Geophys. Res. 66, 2607-2640 (1961).

Farley, T. A., "The growth of our knowledge of the earth's outer radiation belt," Rev. Geophys. 1, 3-34 (1963).

Farley, T. A., and A. Rosen, "Charged-particle variations in the outer Van Allen zone during a geomagnetic storm," J. Geophys. Res. 65, 3494-3496 (1960).

Farley, T. A., and N. L. Sanders, "Pitch angle distributions and mirror point densities in the outer radiation zone," J. Geophys. Res. 67, 2159-2168 (1962).

Forbush, S. E., G. Pizzella, and D. Venkatesan, "The morphology and temporal variations of the Van Allen radiation belt, October 1959 to December 1960," J. Geophys. Res. 67, 3651-3668 (1962).

Frank, L. A., "Inward radial diffusion of electrons of greater than 1.6 million electron volts in the outer radiation zone," J. Geophys. Res. 70, 3533-3540 (1965a).

Frank, L. A., "On the local-time dependence of outer radiation zone electron ($E > 1.6$ MeV) intensities near the magnetic equator," J. Geophys. Res. 70, 4131-4138 (1965b).

Frank, L. A., "Explorer 12 observations of the temporal variations of low-energy electron intensities in the outer radiation zone during geomagnetic storms," J. Geophys. Res. 71, 4631-4639 (1966).

Frank, L. A., "On the extraterrestrial ring current during geomagnetic storms," J. Geophys. Res. (to be published), (1967).

Frank, L. A., and J. A. Van Allen, "Intensity of electrons in the earth's inner radiation zone," J. Geophys. Res. 68, 1203-1207 (1963).

Frank, L. A., and J. A. Van Allen, "A survey of magnetospheric boundary phenomena," in Research in Geophysics, Vol. 1, Sun, Upper Atmosphere, and Space, ed. Odishaw (Massachusetts Institute of Technology Press, Cambridge, Mass., 1964), pp. 161-187.

Frank, L. A., and J. A. Van Allen, "Correlation of outer radiation zone electrons ($E_e \sim 1$ MeV) with the solar activity cycle," J. Geophys. Res. 71, 2697-2700 (1966).

Frank, L. A., J. A. Van Allen, and H. K. Hills, "A study of charged particles in the earth's outer radiation zone with Explorer 14," J. Geophys. Res. 69, 2171-2192 (1964).

Frank, L. A., J. A. Van Allen, J. D. Craven, and H. K. Hills, "Measurements of low-energy charged particle intensities at low altitudes with Injun 4," Trans. Am. Geophys. Union 46, 140 (Abstract), (1965).

Herlofson, N., "Diffusion of particles in the earth's radiation belts," Phys. Rev. Letters 5, 414-416 (1960).

Hess, W. N., G. D. Mead, and M. P. Nakada, "Advances in particles and field research in the satellite era," Rev. Geophys. 3, 521-570 (1965).

Hills, H. Kent, "Observations of electron intensities in the outer radiation zone with OGO 1," Trans. Am. Geophys. Union 48, 163 (Abstract), (1967).

Hoffman, R. A., R. L. Arnoldy, and J. R. Winckler, "Observations of the Van Allen radiation regions during August and September 1959, 6, properties of the outer region," J. Geophys. Res. 67, 4543-4576 (1962).

Kellogg, P. J., "Van Allen radiation of solar origin," Nature 183, 1295-1297 (1959).

Kennel, C. F., and H. E. Petschek, "Limit on stably trapped particle fluxes," J. Geophys. Res. 71, 1-28 (1966).

Krymov, Yu. S., and B. A. Tverskoy, "Alteration of particle energy in a dipole field in transitions between different drift surfaces," Geomagnetism and Aeronomy 4, 309-311 (1964).

Lew, John S., "Drift rate in a dipole field," J. Geophys. Res. 66, 2681-2685 (1961).

McIlwain, Carl E., "Coordinates for mapping the distribution of magnetically trapped particles," J. Geophys. Res. 66, 3681-3692 (1961).

McIlwain, C. E., "The radiation belts, natural and artificial," Science 142, 355-361 (1963).

McIlwain, Carl E., "Ring current effects on trapped particles," J. Geophys. Res. 71, 3623-3628 (1966a).

McIlwain, C. E., "Processes acting upon outer zone electrons I. Adiabatic perturbations," Univ. of California at San Diego Report UCSD-SP-66-5 (1966b).

Mihalov, J. D., and R. Stephen White, "Energetic electron spectra in the radiation belts," J. Geophys. Res. 71, 2217-2226 (1966).

Nakada, M. P., and G. D. Mead, "Diffusion of protons in the outer radiation belt," J. Geophys. Res. 70, 4777-4792 (1965).

Nakada, M. P., J. W. Dungey, and W. N. Hess, "On the origin of outer-belt protons, 1," J. Geophys. Res. 70, 3529-3532 (1965).

Northrop, Theodore G., "Adiabatic charged-particle motion," Rev. Geophys. 1, 283-304 (1963).

Northrop, Theodore G., and Edward Teller, "Stability of the adiabatic motion of charged particles in the earth's field," Phys. Rev. 117, 215-225 (1960).

Parker, E. N., "Geomagnetic fluctuations and the form of the outer zone of the Van Allen radiation belt," J. Geophys. Res. 65, 3117-3130 (1960).

Pfitzer, Karl, Sharad Kane, and John R. Winckler, "The spectra and intensity of electrons in the radiation belts," Space Research 6, 702-713 (1966).

Pizzella, G., L. R. Davis, and J. M. Williamson, "Electrons in the Van Allen zone measured with a scintillator on Explorer 14," J. Geophys. Res. 71, 5495-5508 (1966).

Ray, Ernest C., "On the application of Liouville's theorem to the intensity of radiation trapped in the geomagnetic field," *Univ. of Iowa Research Report 59-21* (1959).

Rosser, W. G. V., B. J. O'Brien, J. A. Van Allen, L. A. Frank, and C. D. Laughlin, "Electrons in the earth's outer radiation zone," J. Geophys. Res. 67, 4533-4542 (1962).

Roederer, Juan G., "On the adiabatic motion of energetic particles in a model magnetosphere," J. Geophys. Res. 72, 981-992 (1967).

Serlemitsos, P., "Low-energy electrons in the dark magnetosphere," J. Geophys. Res. 71, 61-77 (1966).

Shabansky, V. P., "Radiation belts," Geomagnetism and Aeronomy 5, 765-789 (1965).

Störmer, C., *The Polar Aurora* (Oxford, Clarendon Press, 1955).

Sugiura, M., "Hourly values of equatorial D_{ST} for the IGY," Ann. Intern. Geophys. Yr. 35, 9-45 (1964).

Taylor, Harold E., "Adiabatic motion of outer-zone particles in a model of the geoelectric and geomagnetic fields," J. Geophys. Res. 71, 5135-5148 (1966).

Tverskoy, B. A., "Dynamics of the radiation belts of the earth, II," Geomagnetism and Aeronomy 4, 351-366 (1964).

Tverskoy, B. A., "Transport and acceleration of charged particles in the earth's magnetosphere," Geomagnetism and Aeronomy 5, 617-628 (1965).

Vette, J. I., "Trapped radiation model environments," Geophysics and Space Data Bulletin, ed. Carrigan and Oliver, Vol. II, No. 4, pp. 207-315 (1965).

Williams, Donald J., "A 27-day periodicity in outer zone trapped electron intensities," J. Geophys. Res. 71, 1815-1826 (1966).

Williams, D. J., and W. F. Palmer, "Distortions in the radiation cavity as measured by an 1100-kilometer polar orbiting satellite," J. Geophys. Res. 70, 557-568 (1965).

Williams, D. J., and A. M. Smith, "Daytime trapped electron intensities at high latitudes at 1100 kilometers," J. Geophys. Res. 70, 541-556 (1965).

FIGURE CAPTIONS

Figure 1	Projection of the orbit onto the solar ecliptic equatorial plane. The shaded area designates the region traversed during the period 5 September through 31 December, 1964.
Figure 2	Projection of the orbit onto the solar ecliptic meridian plane passing through apogee.
Figure 3	A view of the experiment package and the array of detectors. The spacecraft spins approximately about the Z axis, which is normal to the plane of the figure.
Figure 4	The path, in celestial coordinates, of the centers of the fields of view of detectors A1, B1, and H.
Figure 5	A machine plot of the detector counting rates as functions of geocentric radial distance for the low-latitude inbound pass of October 17, 1964.
Figure 6	A machine plot showing energy spectrum indices, counting rate, and pitch angle parameters as functions of L, for a representative pass. See the text for explanation.

Figure 7	Contours of constant intensity of electrons ($E > 40$ keV) in (L, time) space, as measured with detector A1. Proton contributions to the counting rate at $L \lesssim 4$ have been eliminated. The average (over two days) of K_p daily sums is shown in the lower portion of the figure.
Figure 8	Continuation of Figure 7 for the responses of detector B2.
Figure 9	Continuation of Figure 7 for the responses of detector C. The proton contribution to the counting rate of the detector was negligible.
Figure 10	The omnidirectional intensities at $L = 3$ of electrons of energies $E > 40$ keV, $E > 130$ keV, and $E > 2$ MeV, displayed as a function of time. The average (over two days) daily K_p sum is also exhibited.
Figure 11	Continuation of Figure 10 for the intensities at $L = 5$.
Figure 12	Continuation of Figure 10 for the intensities at $L = 7$.
Figure 13	The equatorial plane magnetic field perturbation used in the calculations. $\Delta B(L)$ is the deviation from the dipole field $B_o = .312/L^3$ and is shown for several values of $D_{ST}(H)$.

Figure 14 $D_{ST}(H)$ hourly average for the magnetic storm of November 1, 1964.

Figure 15 Smoothed version of the $D_{ST}(H)$ profile in Figure 14, used in computing the effects of magnetic storms on charged particle intensities.

Figure 16 Computed dependence of equatorial locations of particles on $D_{ST}(H)$. Adiabatic motion was assumed.

Figure 17 Predicted dependence of the intensity of electrons ($E > 40$ keV) measured with detector A1 on $D_{ST}(H)$, normalized to the intensity when $D_{ST}(H) = -9\ \gamma$.

Figure 18 Continuation of Figure 17 for the intensity of electrons ($E > 130$ keV) measured with detector B2.

Figure 19 Continuation of Figure 17 for the intensity of electrons ($E > 2$ MeV) measured with detector C.

Figure 20 Predicted contours of constant intensity measured by detector A1. Calculations were based on the radial intensity dependence observed on October 31, 1964, and on the $D_{ST}(H)$ profile shown in Figure 15. Contour labels are in counts $\sec^{-1}$.

Figure 21 Continuation of Figure 20 for the predicted intensity measured by detector B2.

Figure 22	Continuation of Figure 20 for the predicted intensity measured by detector C.
Figure 23	Diagrams illustrating the application of the spherical harmonic addition theorem to the geometry of the directional detector orientation.
Figure 24	Dependence of the calculated modulation (defined as the maximum counting rate in a spin cycle divided by the minimum) on n and Γ for a $\sin^n\alpha$ angular distribution and the measured angular response function of the detector. Γ is the angle between the spin vector and the magnetic field.
Figure 25	Illustrations of the detector orientations with respect to the magnetic field direction.
Figure 26	The time interval separating detector crossings of the plane perpendicular to the magnetic field, as a function of Γ. When the particle pitch angle distributions are peaked perpendicular to the field, this time is also the time interval separating the counting rate peaks in the spin modulation.

Figure 27 The omnidirectional multiplier $\frac{1}{G_{mo}}$ and the directional multiplier $\frac{1}{g_m}$, both for use with the maximum counting rate of detector A1 in a spin cycle. See Appendix II for further details.

Figure 28 Continuation of Figure 27 for use with detector B2.

Figure 29 Illustration of the validity of using the sum of the counting rates of three mutually orthogonal detectors as a measure of the omnidirectional intensity. The counting rate of an individual detector is included for comparison, as well as the calculated counting rate.

G 66-887

OGO I TRAJECTORY
SOLAR ECLIPTIC COORDINATES
EQUATORIAL PLANE PROJECTION
SEPTEMBER-DECEMBER, 1964

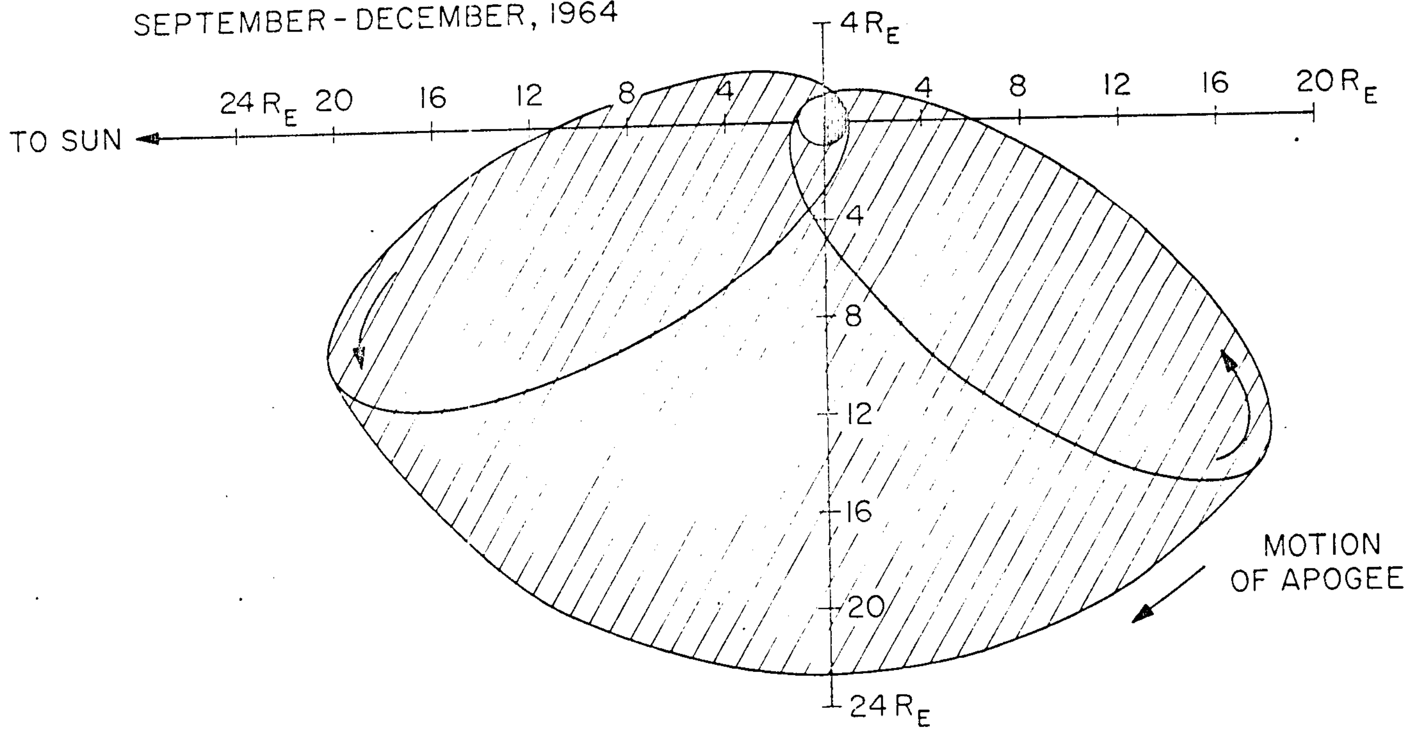

FIGURE 1

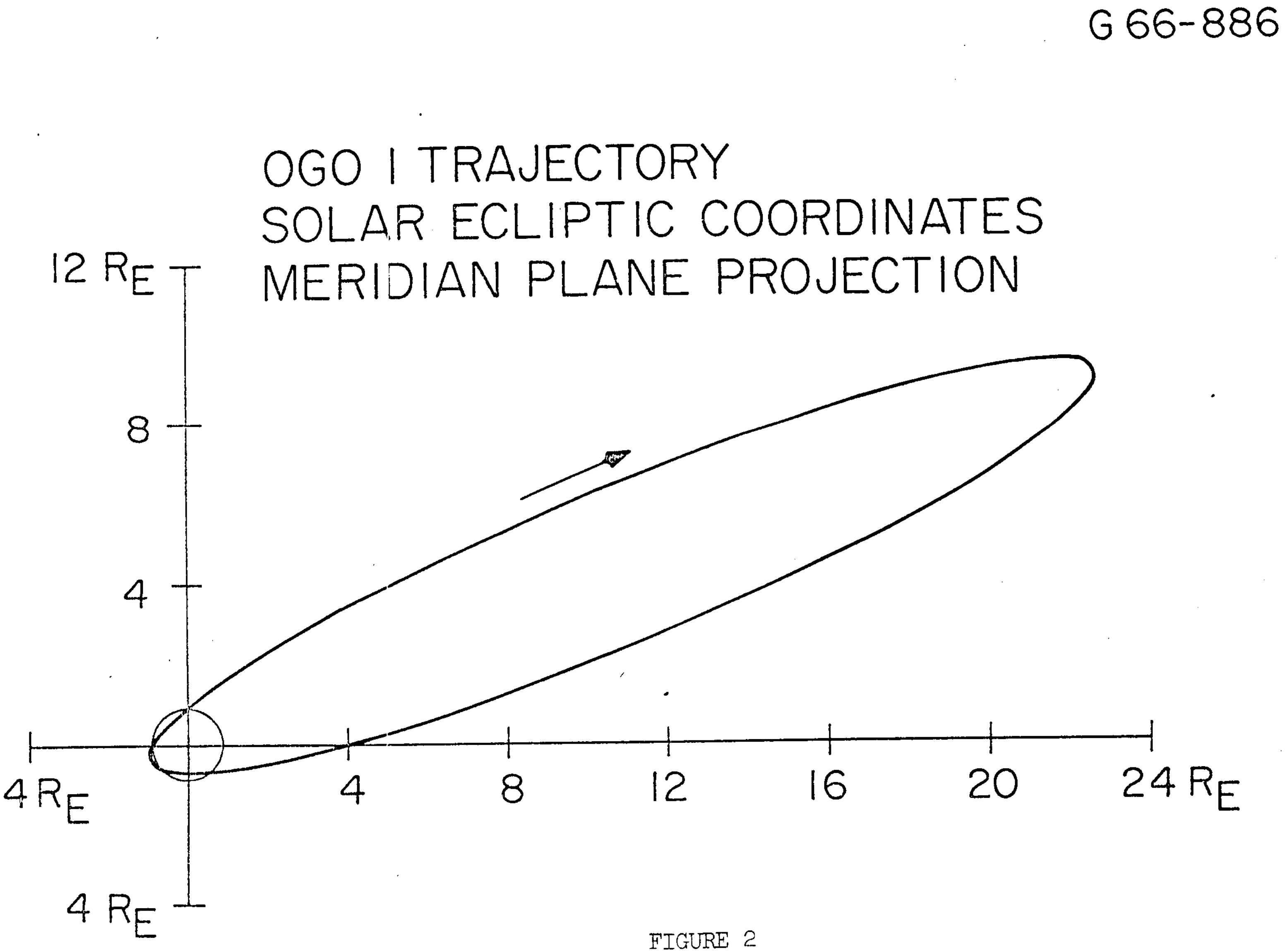
G 66-886
OGO I TRAJECTORY
SOLAR ECLIPTIC COORDINATES
MERIDIAN PLANE PROJECTION
12 R_E
8
4
4 R_E
4 R_E
4
8
12
16
20
24 R_E

FIGURE 2

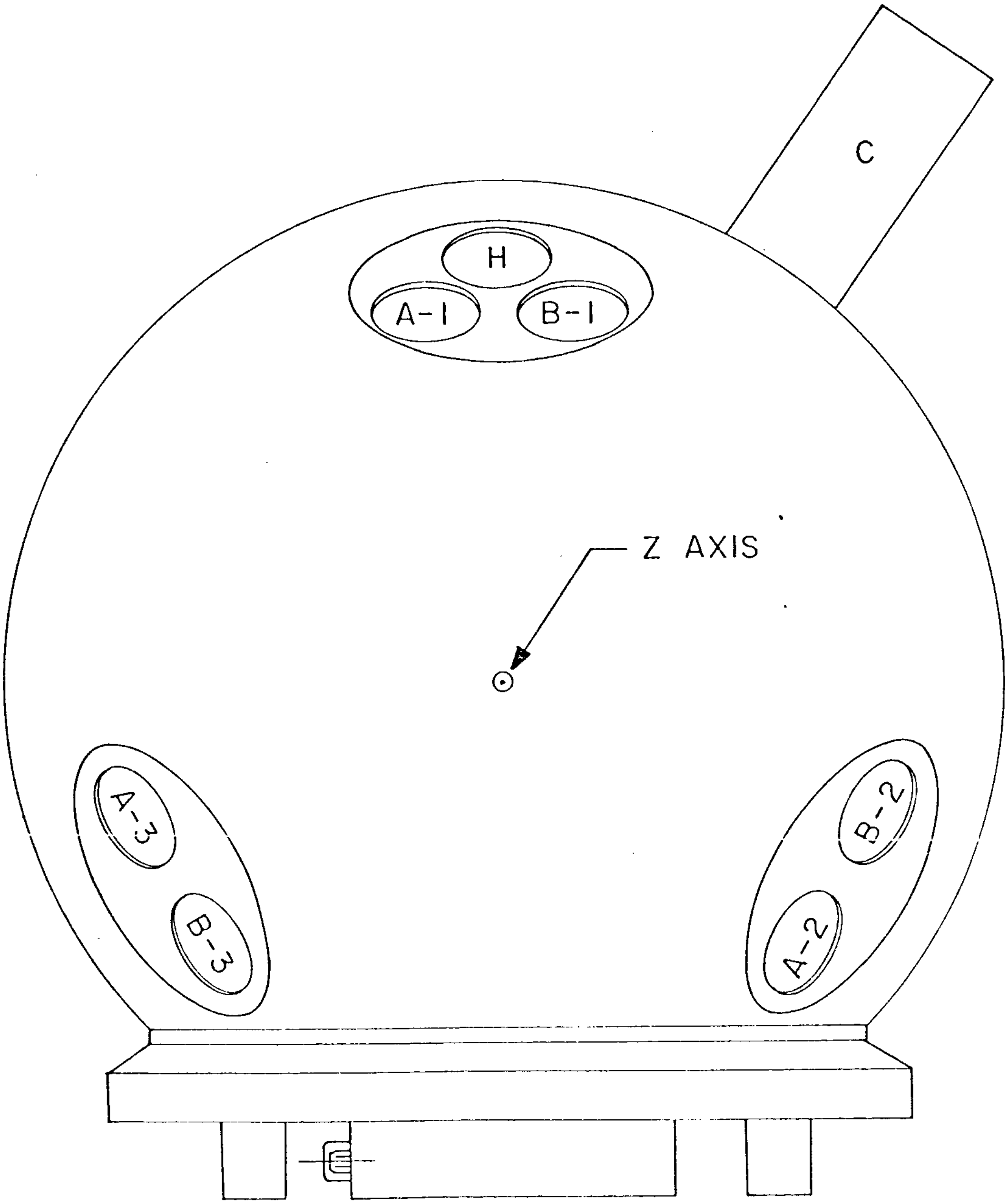

G 67-203

OGO I
UNIVERSITY OF IOWA DETECTORS

FIGURE 3

G66-884

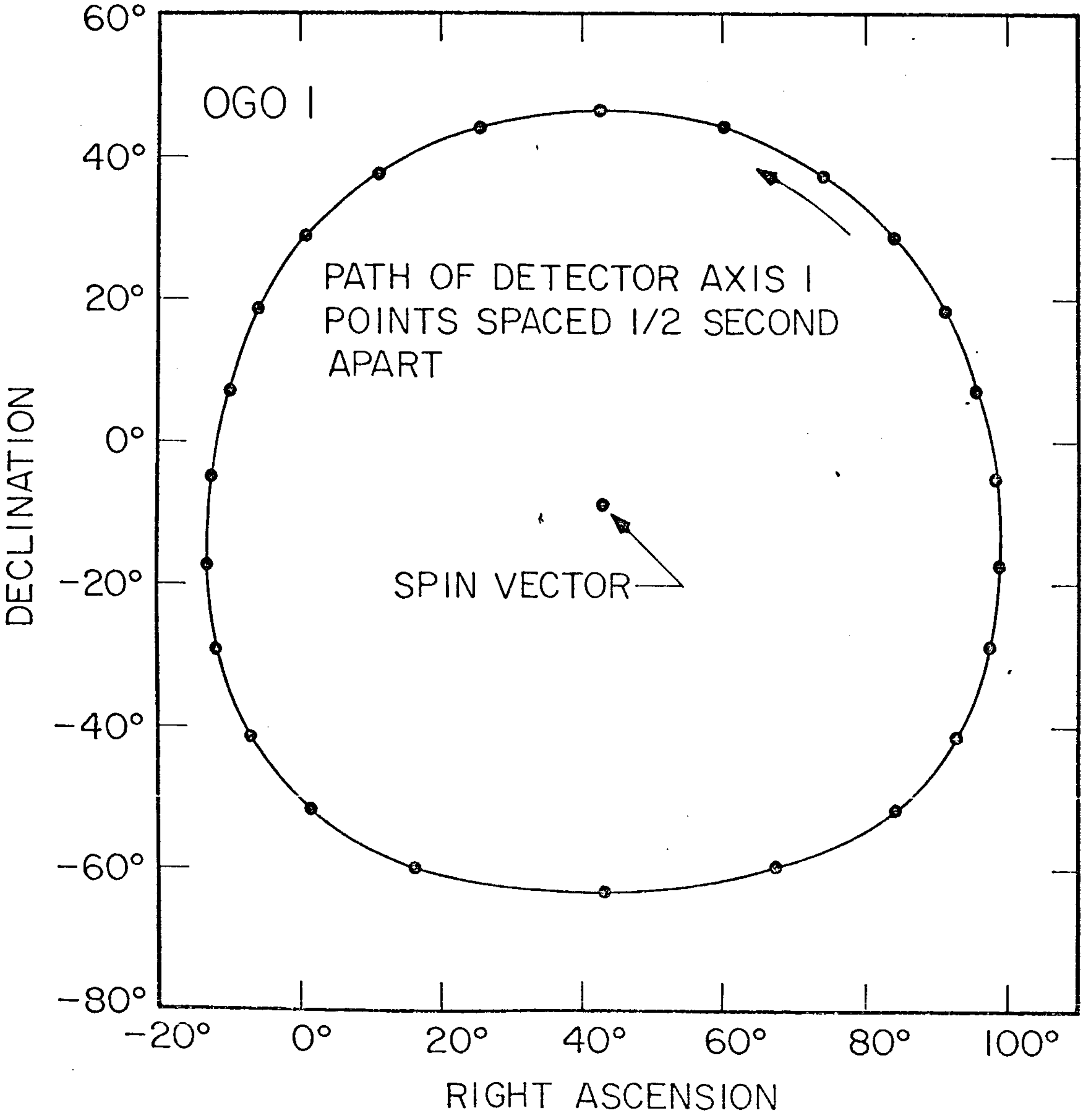

FIGURE 4

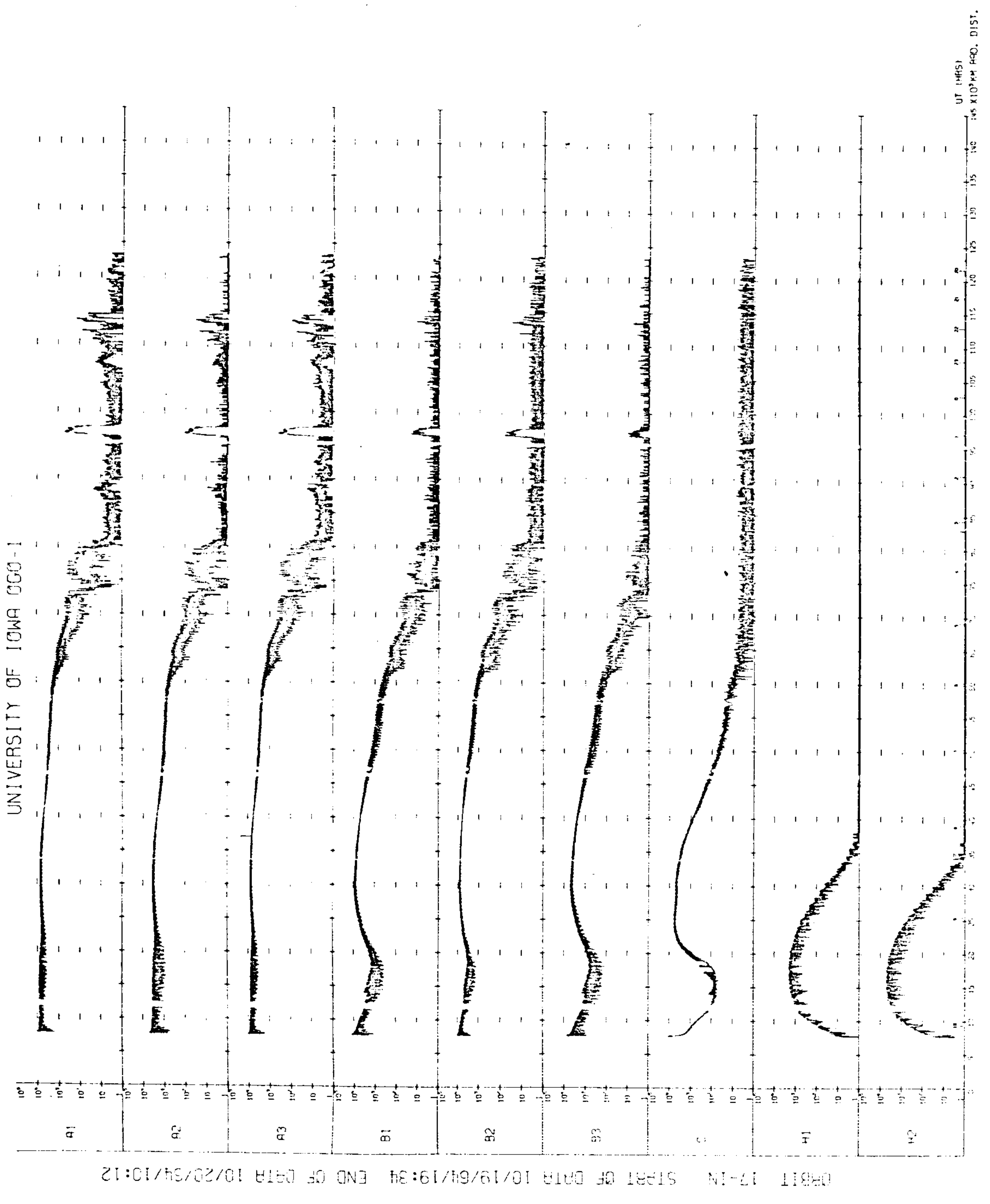
UNIVERSITY OF IOWA OGO-1
A1
A2
A3
B1
B2
B3
C
H1
H2
UT (HRS)
X10³KM APO. DIST.
125
130
135
140
145
ORBIT 17-IN START OF DATA 10/19/64/19:34 END OF DATA 10/20/64/10:12

FIGURE 5

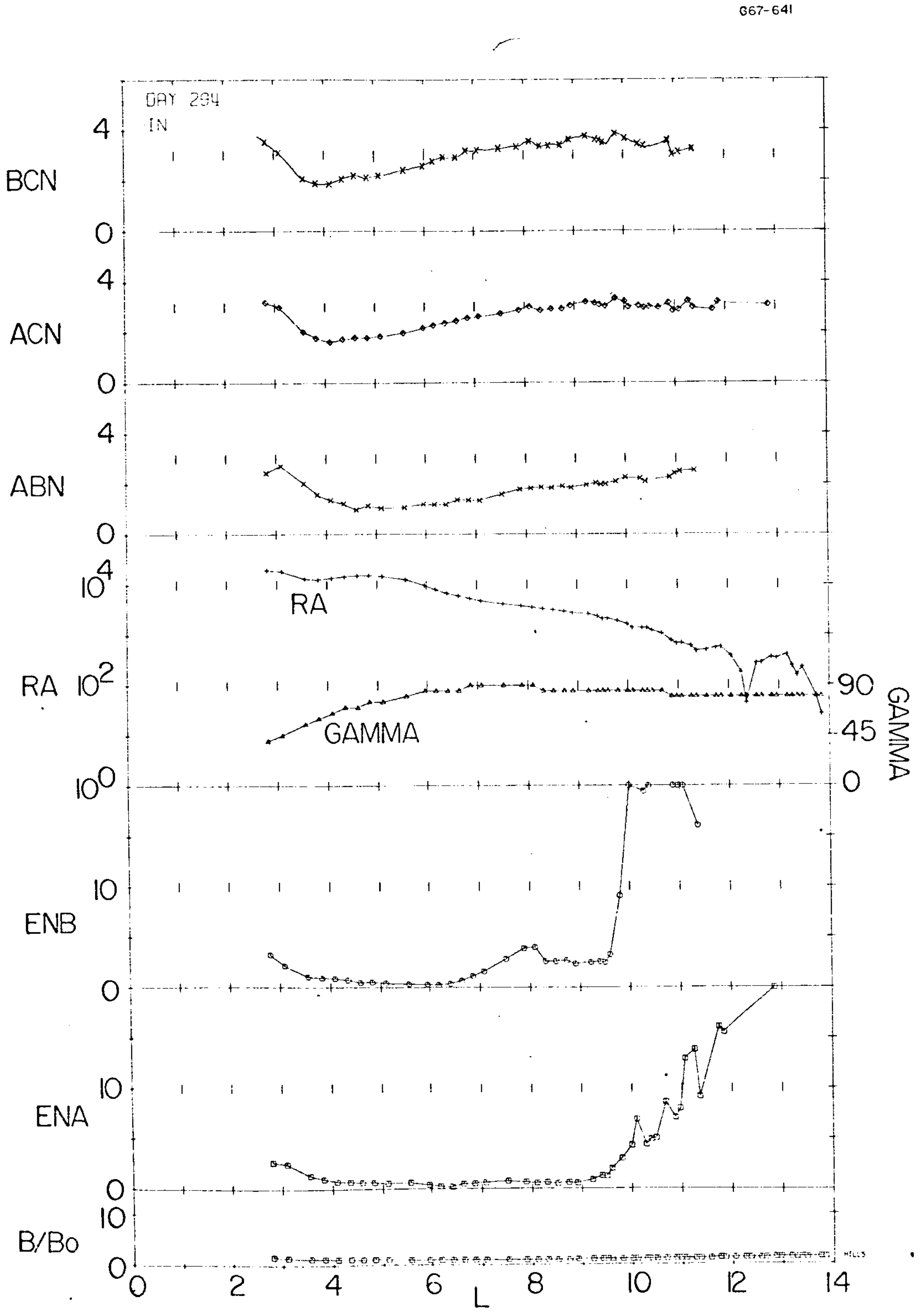
G67-641
DAY 284
IN
BCN
ACN
ABN
RA
GAMMA
ENB
ENA
B/Bo
4
0
10^4
10^2
10^0
90
45
10
0
2
4
6
8
10
12
14
L
HILLS

FIGURE 6

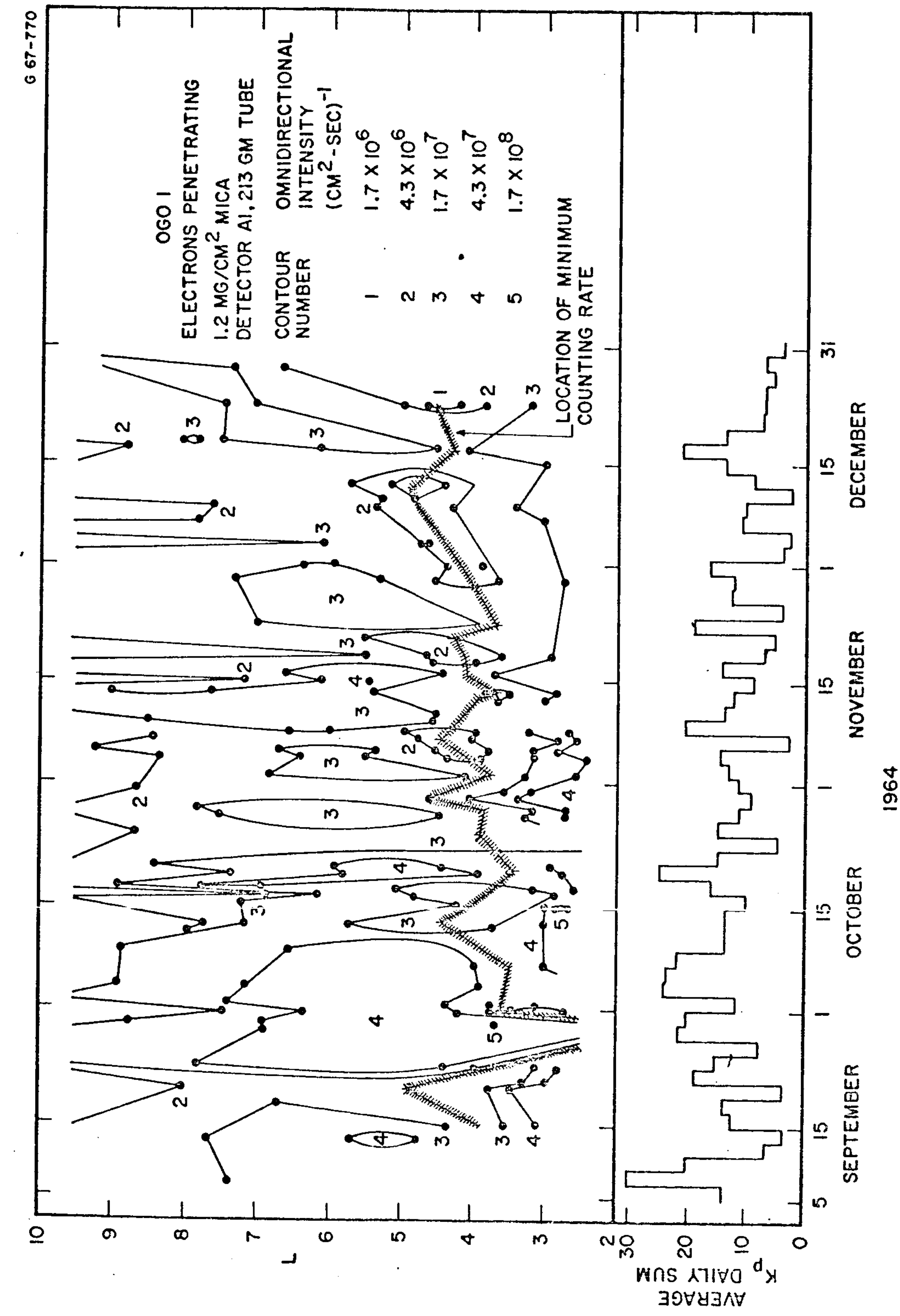
G 67-770
OGO I
ELECTRONS PENETRATING
1.2 MG/CM² MICA
DETECTOR Al, 213 GM TUBE
CONTOUR NUMBER
OMNIDIRECTIONAL INTENSITY (CM²-SEC)⁻¹
1 1.7 X 10⁶
2 4.3 X 10⁶
3 1.7 X 10⁷
4 4.3 X 10⁷
5 1.7 X 10⁸
LOCATION OF MINIMUM COUNTING RATE
L
2
3
4
5
6
7
8
9
10
AVERAGE Kp DAILY SUM
0
10
20
30
5
15
1
15
1
15
1
15
31
SEPTEMBER
OCTOBER
NOVEMBER
DECEMBER
1964

FIGURE 7

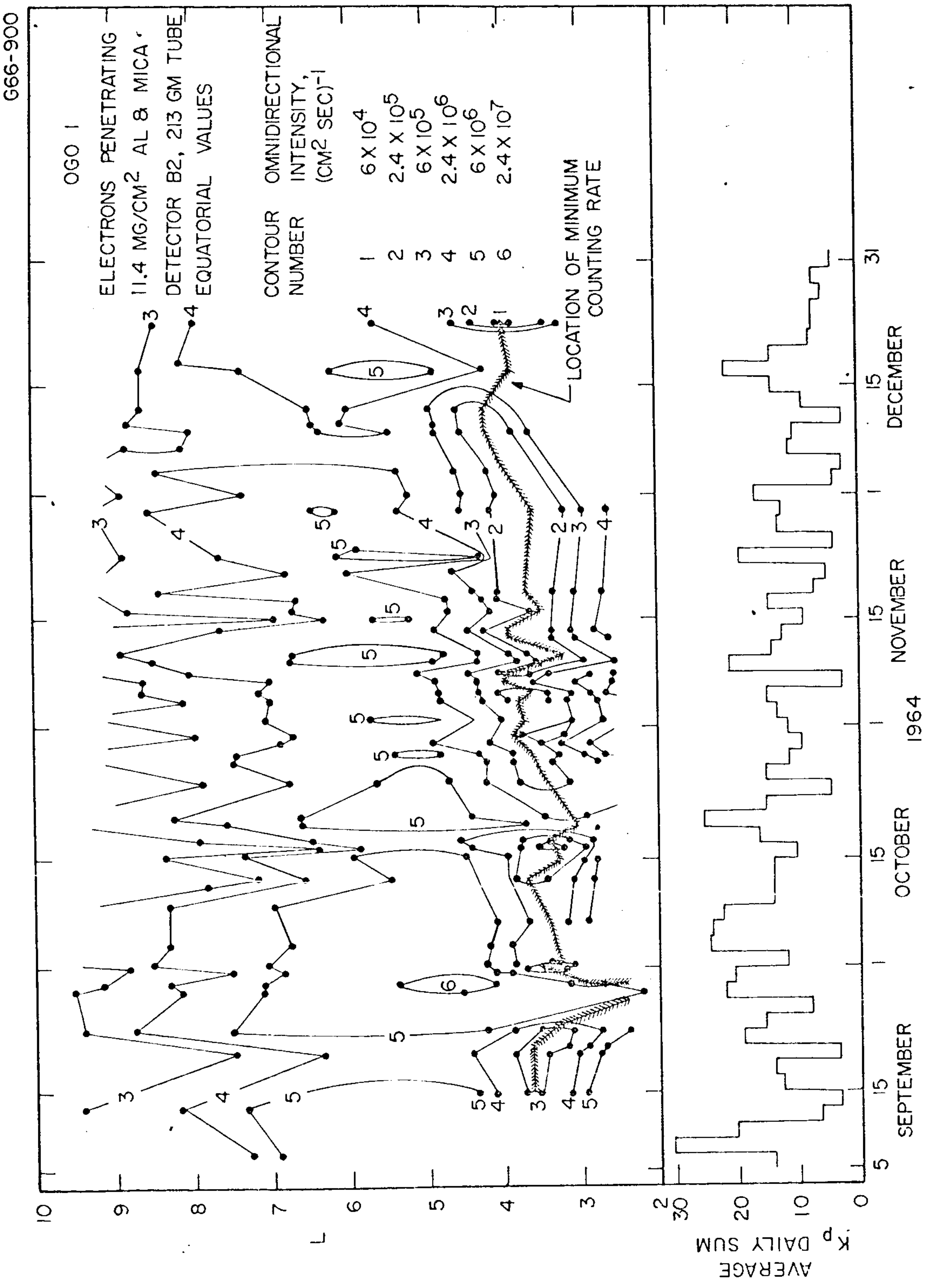
G66-900
OGO I
ELECTRONS PENETRATING
11.4 MG/CM² AL & MICA
DETECTOR B2, 213 GM TUBE
EQUATORIAL VALUES
CONTOUR NUMBER
OMNIDIRECTIONAL INTENSITY, (CM² SEC)⁻¹
1 6 X 10⁴
2 2.4 X 10⁵
3 6 X 10⁵
4 2.4 X 10⁶
5 6 X 10⁶
6 2.4 X 10⁷
LOCATION OF MINIMUM COUNTING RATE
L
2
3
4
5
6
7
8
9
10
AVERAGE Kp DAILY SUM
0
10
20
30
5
15
SEPTEMBER
1
15
OCTOBER
1
15
NOVEMBER
1964
1
15
DECEMBER
31

FIGURE 8

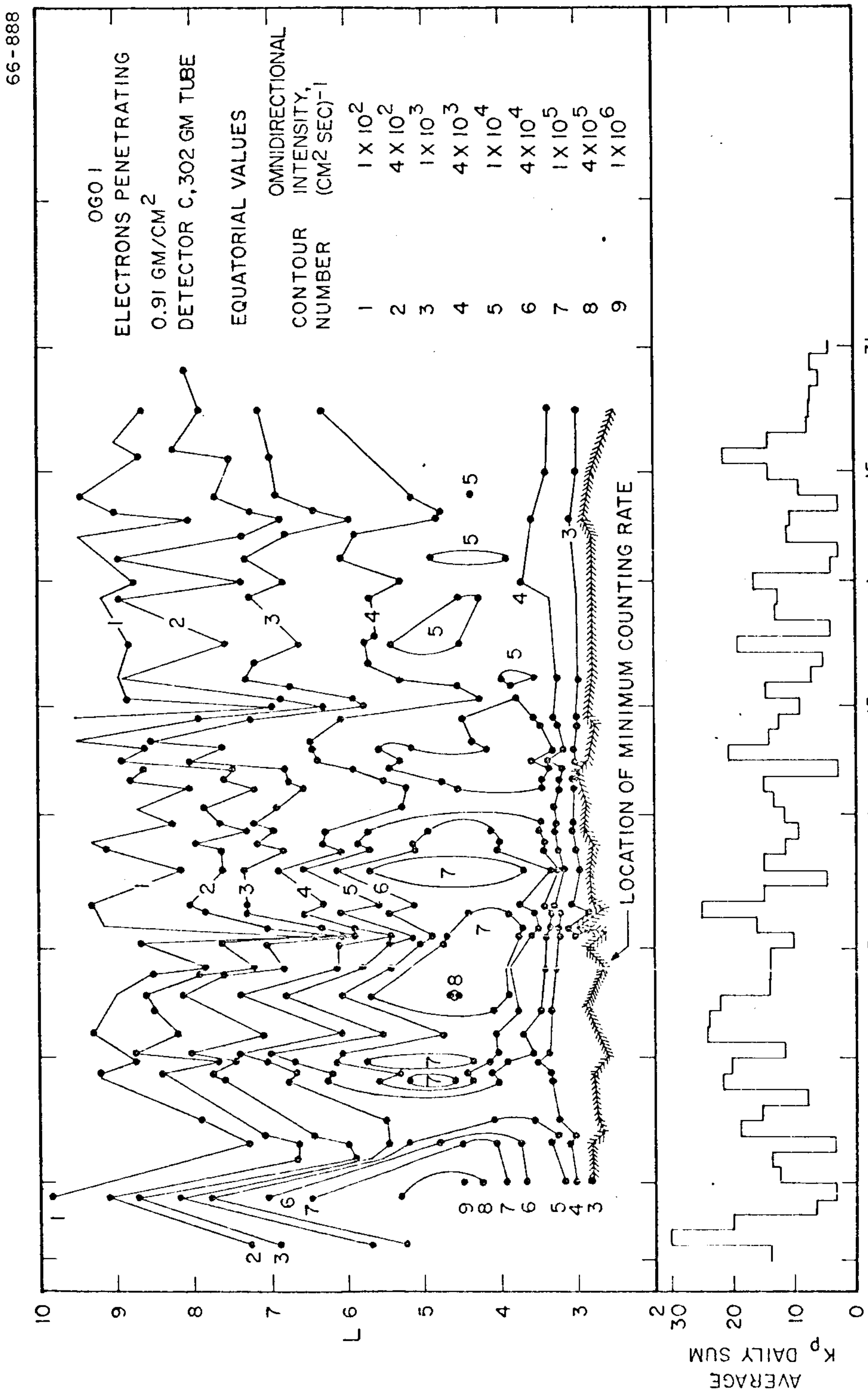
66-888
OGO I
ELECTRONS PENETRATING
0.91 GM/CM^2
DETECTOR C, 302 GM TUBE
EQUATORIAL VALUES
CONTOUR NUMBER
OMNIDIRECTIONAL INTENSITY, (CM^2 SEC)$^{-1}$
1 — 1 X 10^2
2 — 4 X 10^2
3 — 1 X 10^3
4 — 4 X 10^3
5 — 1 X 10^4
6 — 4 X 10^4
7 — 1 X 10^5
8 — 4 X 10^5
9 — 1 X 10^6
LOCATION OF MINIMUM COUNTING RATE
L
10
9
8
7
6
5
4
3
2
AVERAGE K$_p$ DAILY SUM
30
20
10
0
5
15
SEPTEMBER
1
15
OCTOBER
1
15
NOVEMBER
1
15
DECEMBER
31
1964

FIGURE 9

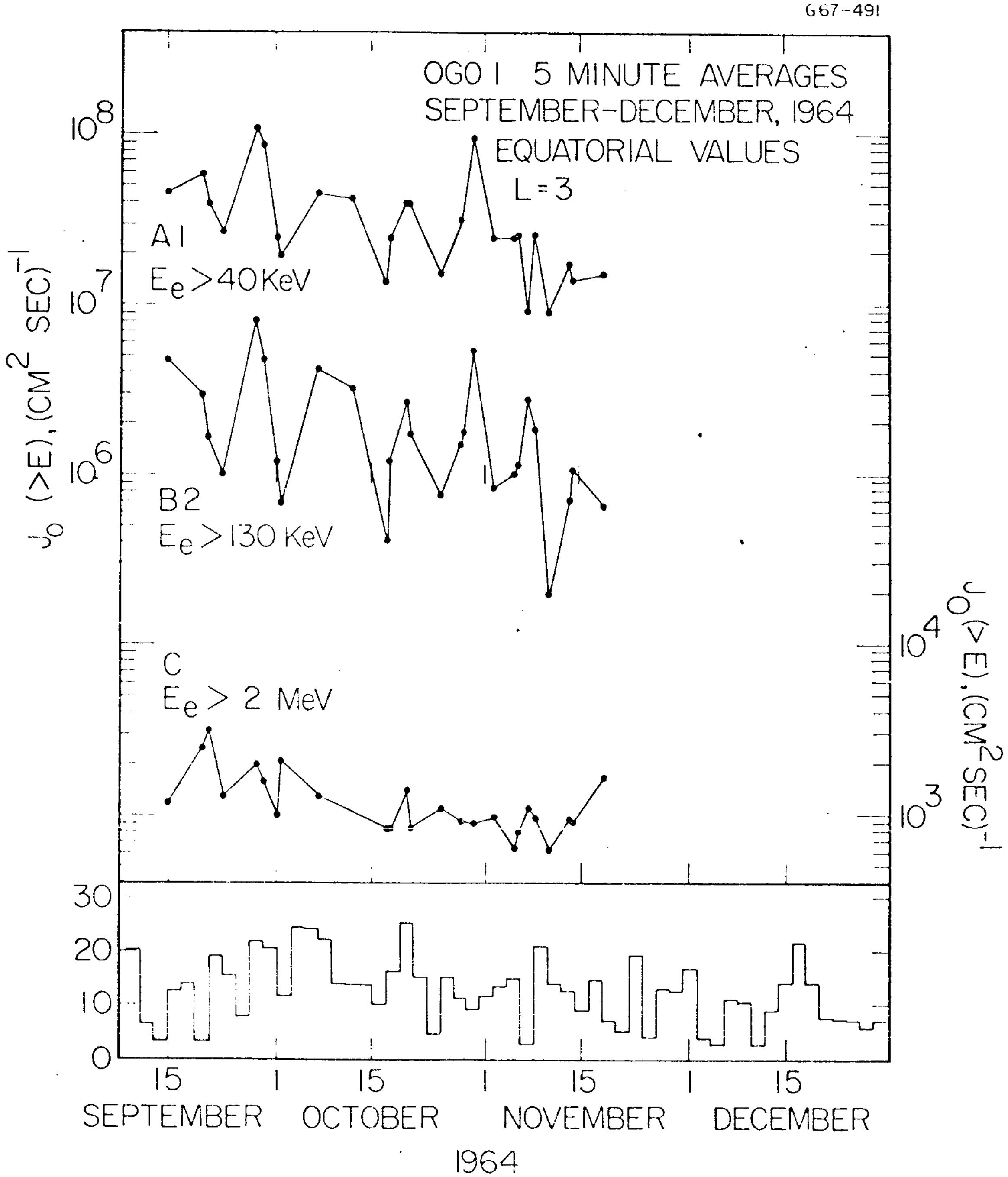
G67-491
OGO I 5 MINUTE AVERAGES
SEPTEMBER-DECEMBER, 1964
EQUATORIAL VALUES
L = 3
A1
E_e > 40 KeV
B2
E_e > 130 KeV
C
E_e > 2 MeV
10^8
10^7
10^6
10^4
10^3
J_0 (>E), (CM^2 SEC)$^{-1}$
J_0 (>E), (CM^2 SEC)$^{-1}$
30
20
10
0
15
1
15
1
15
1
15
SEPTEMBER
OCTOBER
NOVEMBER
DECEMBER
1964

FIGURE 10

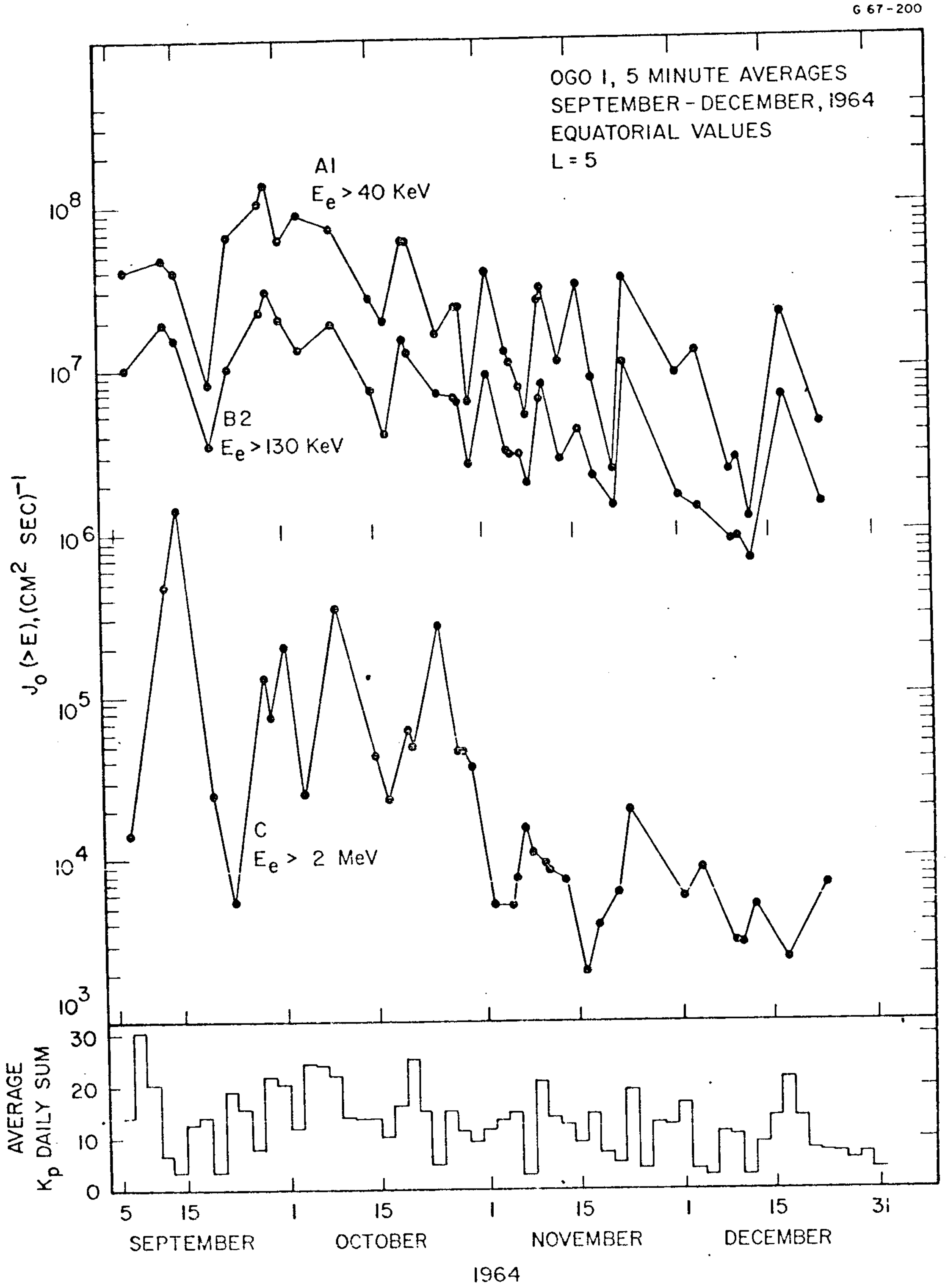
G 67-200
OGO I, 5 MINUTE AVERAGES
SEPTEMBER - DECEMBER, 1964
EQUATORIAL VALUES
L = 5
A1
E_e > 40 KeV
B2
E_e > 130 KeV
C
E_e > 2 MeV
J_o (>E), (CM² SEC)⁻¹
10⁸
10⁷
10⁶
10⁵
10⁴
10³
AVERAGE
K_p DAILY SUM
30
20
10
0
5
15
1
15
1
15
1
15
31
SEPTEMBER
OCTOBER
NOVEMBER
DECEMBER
1964

FIGURE 11

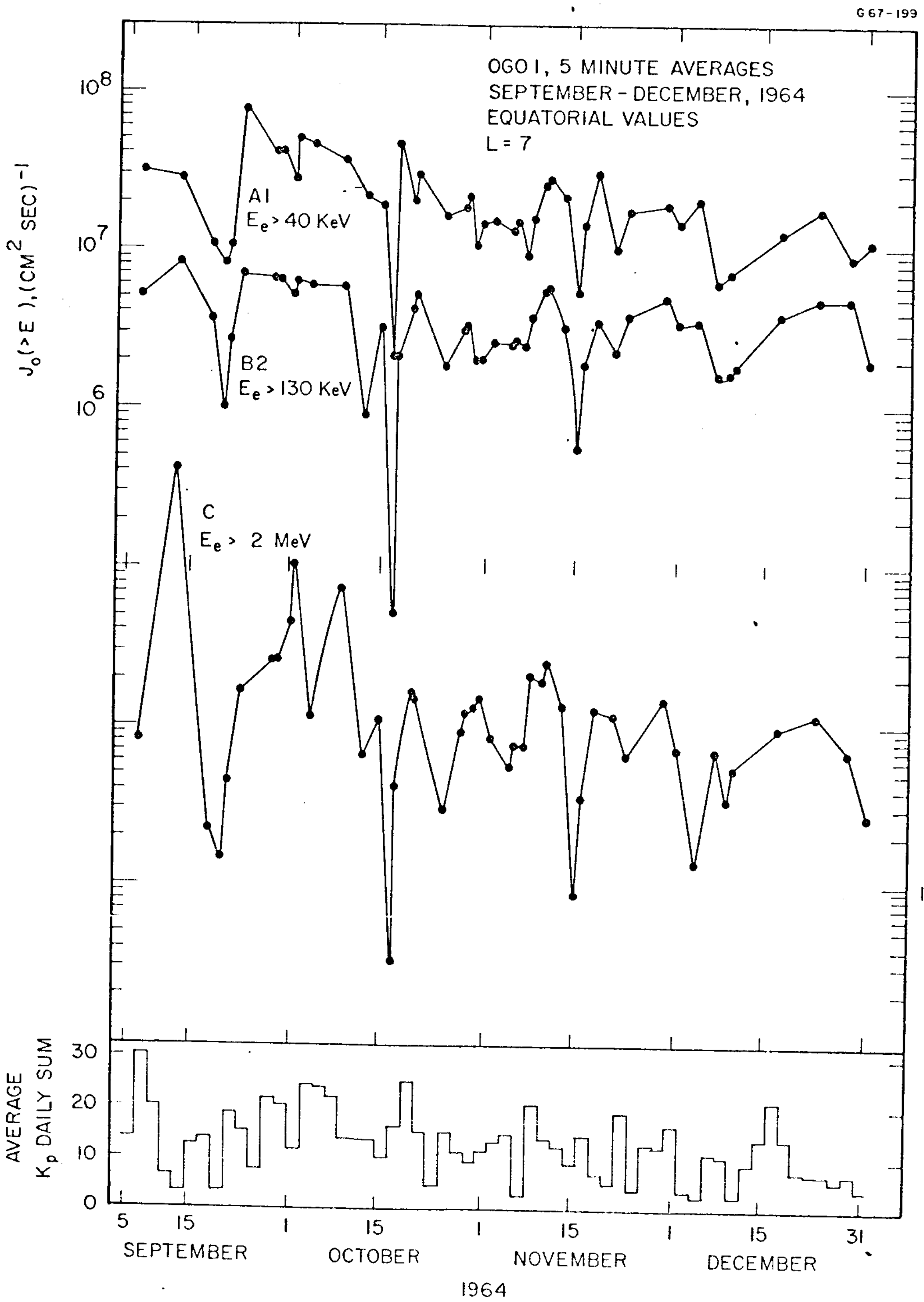
G67-199
OGO I, 5 MINUTE AVERAGES
SEPTEMBER - DECEMBER, 1964
EQUATORIAL VALUES
L = 7
A1
$E_e > 40$ KeV
B2
$E_e > 130$ KeV
C
$E_e > 2$ MeV
$J_o(>E), (CM^2 SEC)^{-1}$
10^8
10^7
10^6
10^5
10^4
10^3
10^2
AVERAGE K_p DAILY SUM
30
20
10
0
5
15
1
15
1
15
1
15
31
SEPTEMBER
OCTOBER
NOVEMBER
DECEMBER
1964

FIGURE 12

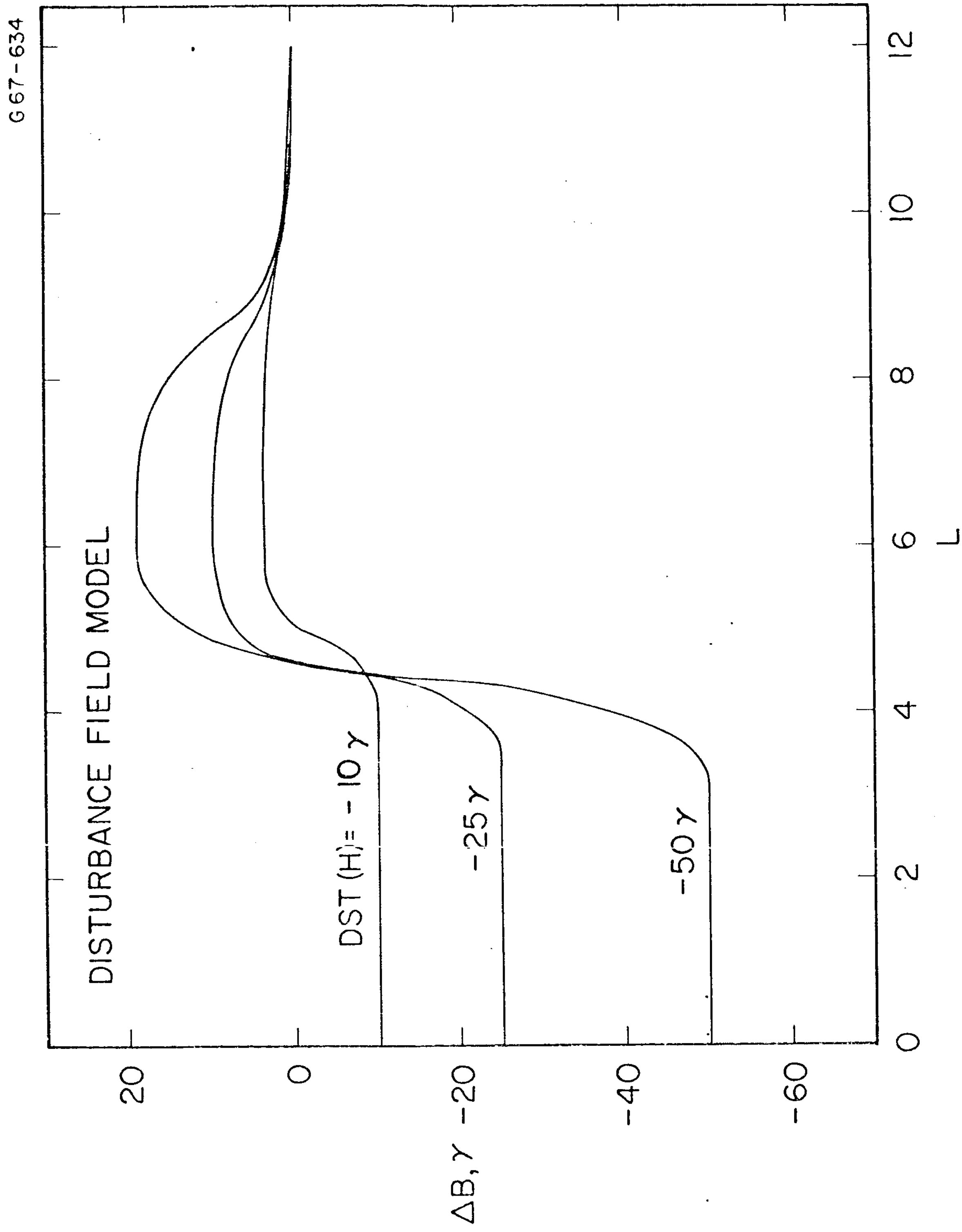
G67-634
DISTURBANCE FIELD MODEL
DST (H) = - 10 γ
-25 γ
-50 γ
$\Delta B, \gamma$
20
0
-20
-40
-60
L
0
2
4
6
8
10
12

FIGURE 13

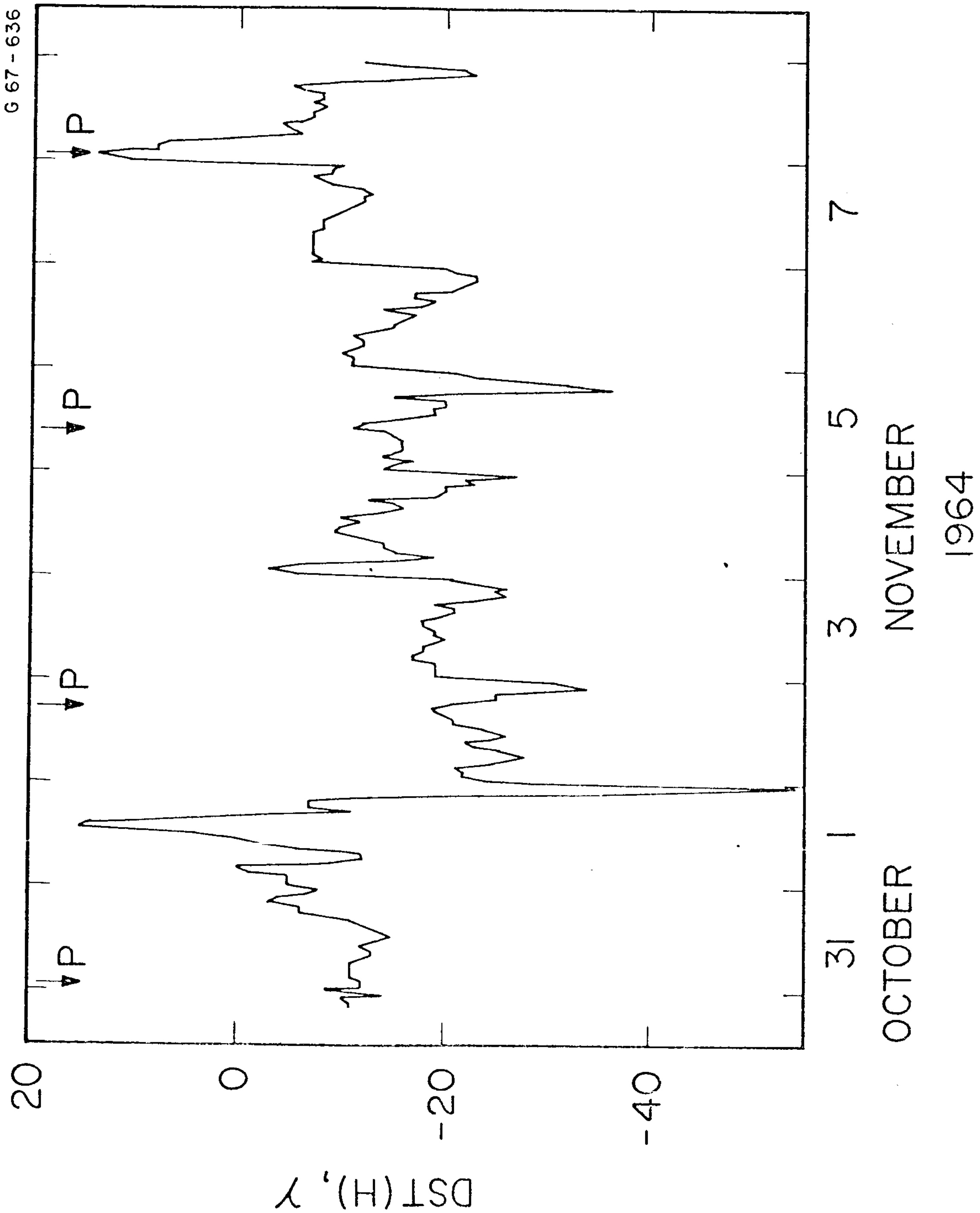

FIGURE 14

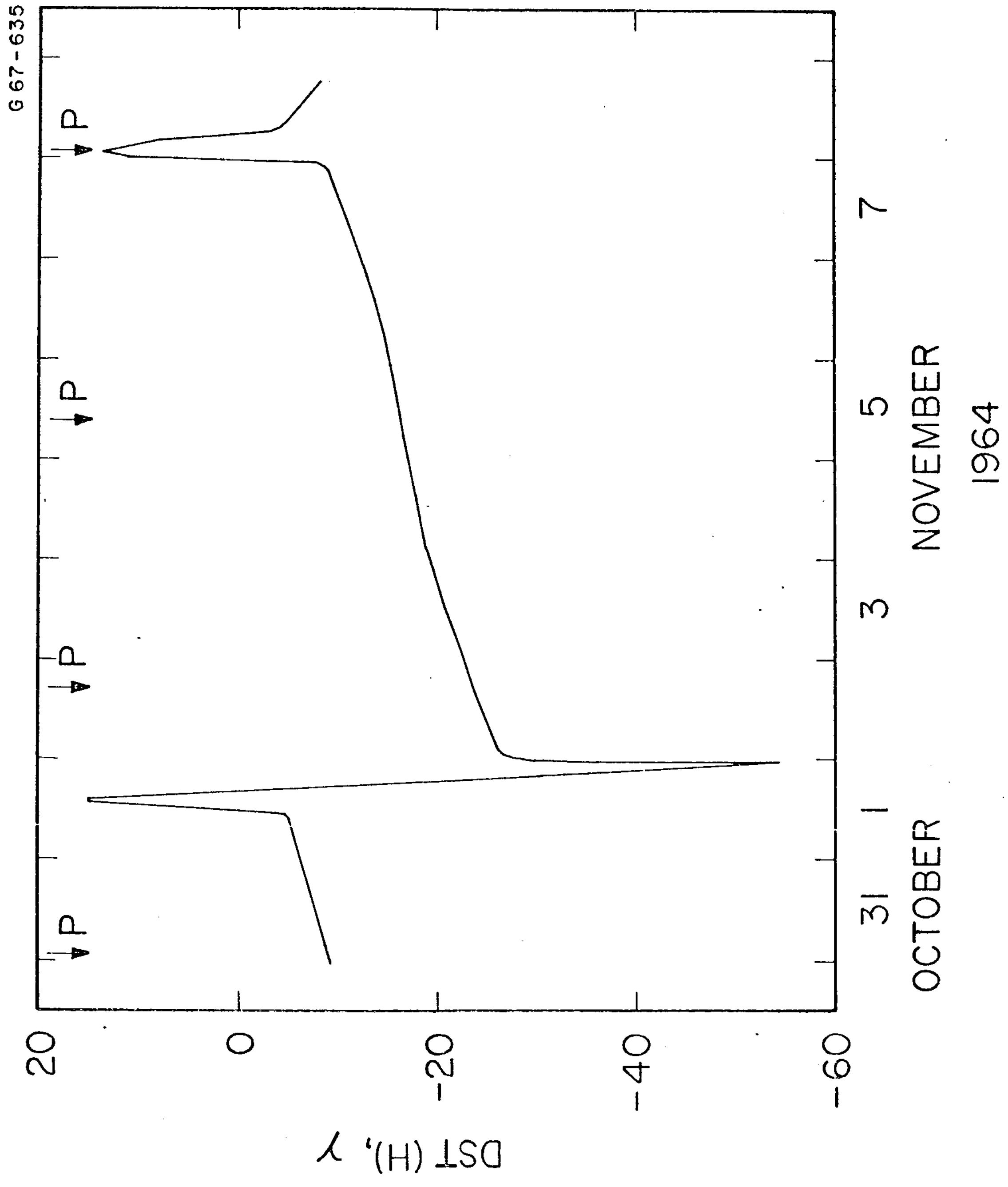

FIGURE 15

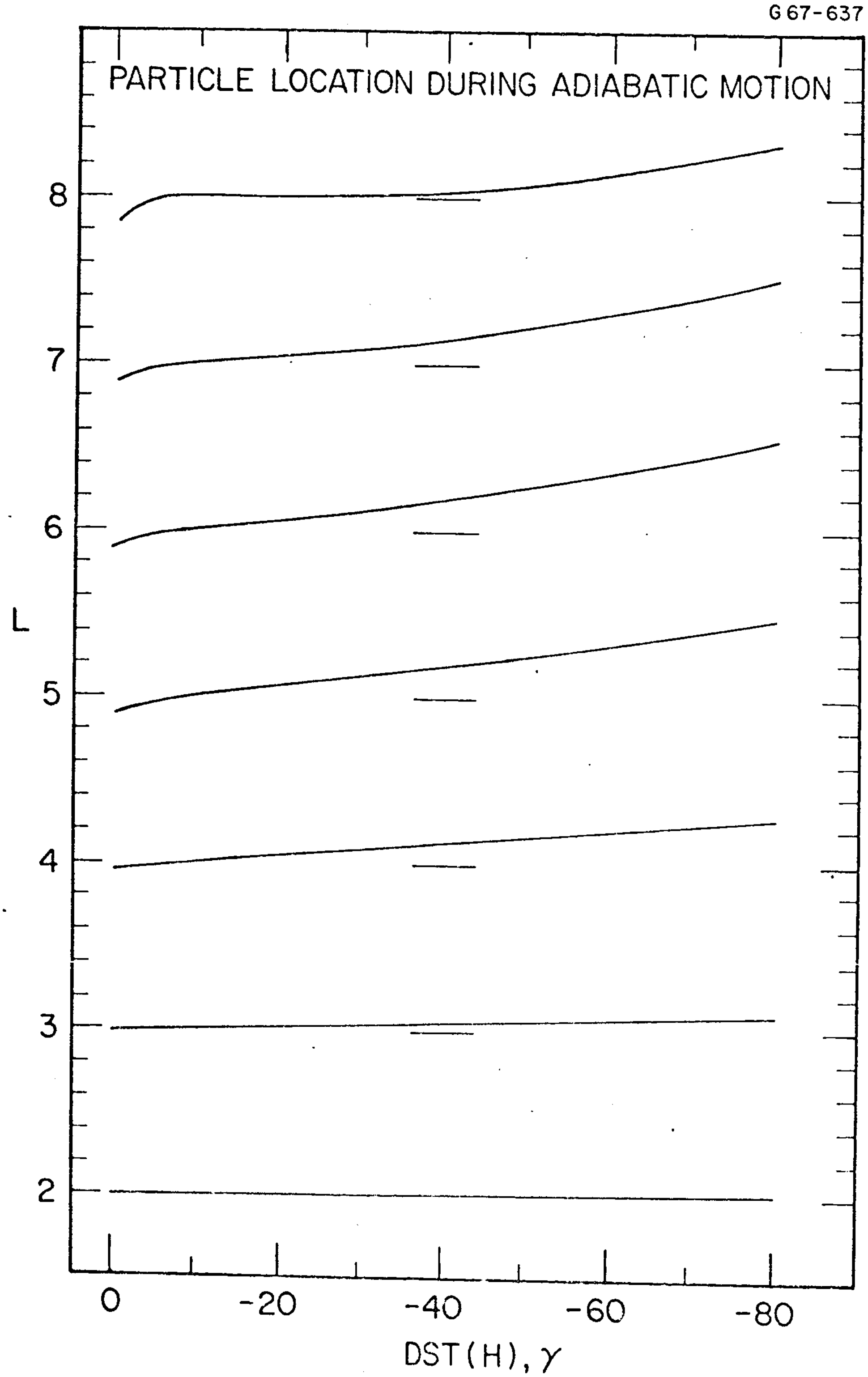
G 67-637
PARTICLE LOCATION DURING ADIABATIC MOTION
L
8
7
6
5
4
3
2
0
-20
-40
-60
-80
DST(H), γ

FIGURE 16

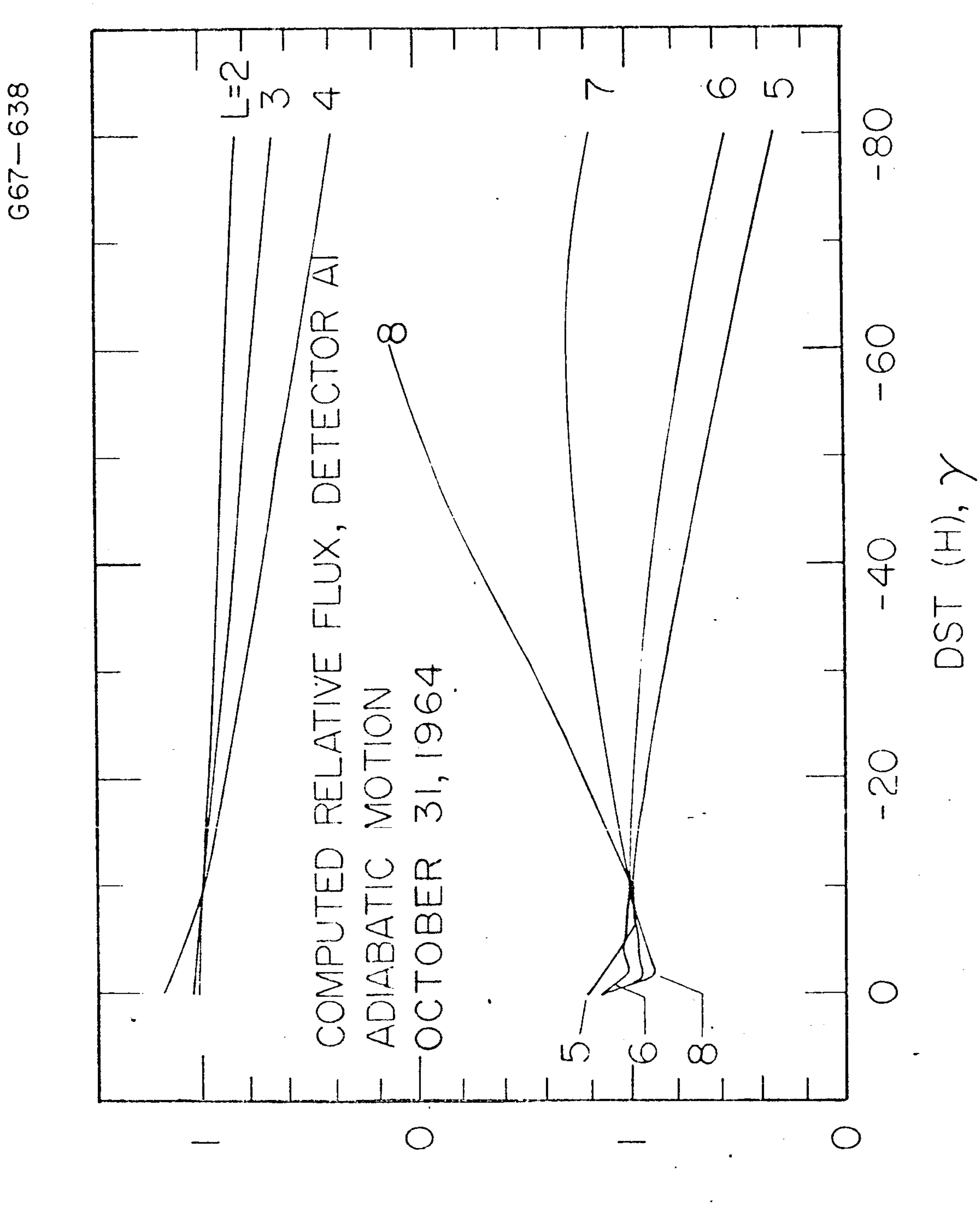
G67—638
COMPUTED RELATIVE FLUX, DETECTOR A1
ADIABATIC MOTION
OCTOBER 31, 1964
L=2
3
4
7
6
5
8
5
6
8
0
-20
-40
-60
-80
DST (H), γ
1
0
1
0

FIGURE 17

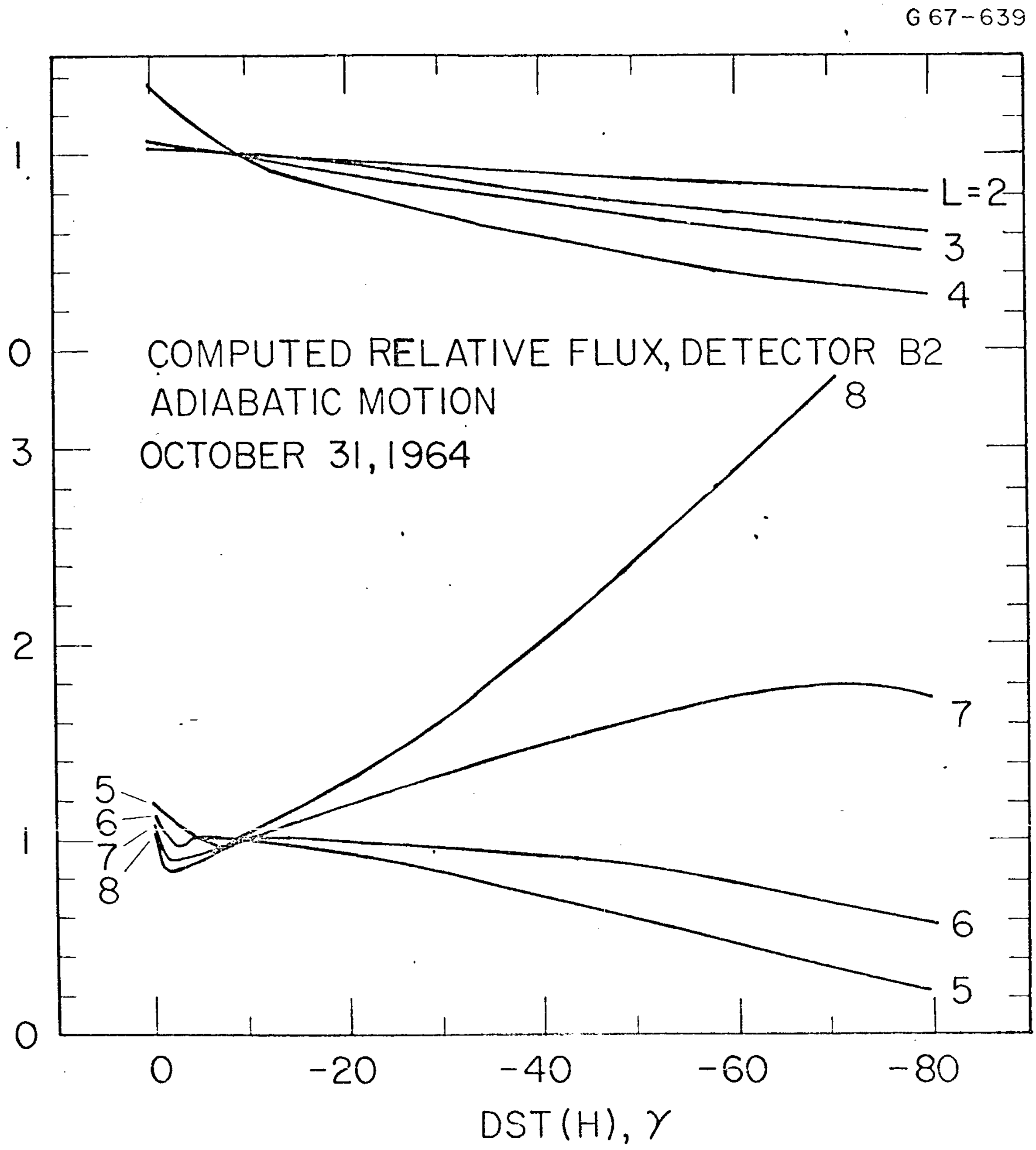
G 67-639
COMPUTED RELATIVE FLUX, DETECTOR B2
ADIABATIC MOTION
OCTOBER 31, 1964
1
0
3
2
1
0
L=2
3
4
8
7
6
5
5
6
7
8
0
-20
-40
-60
-80
DST(H), γ

FIGURE 18

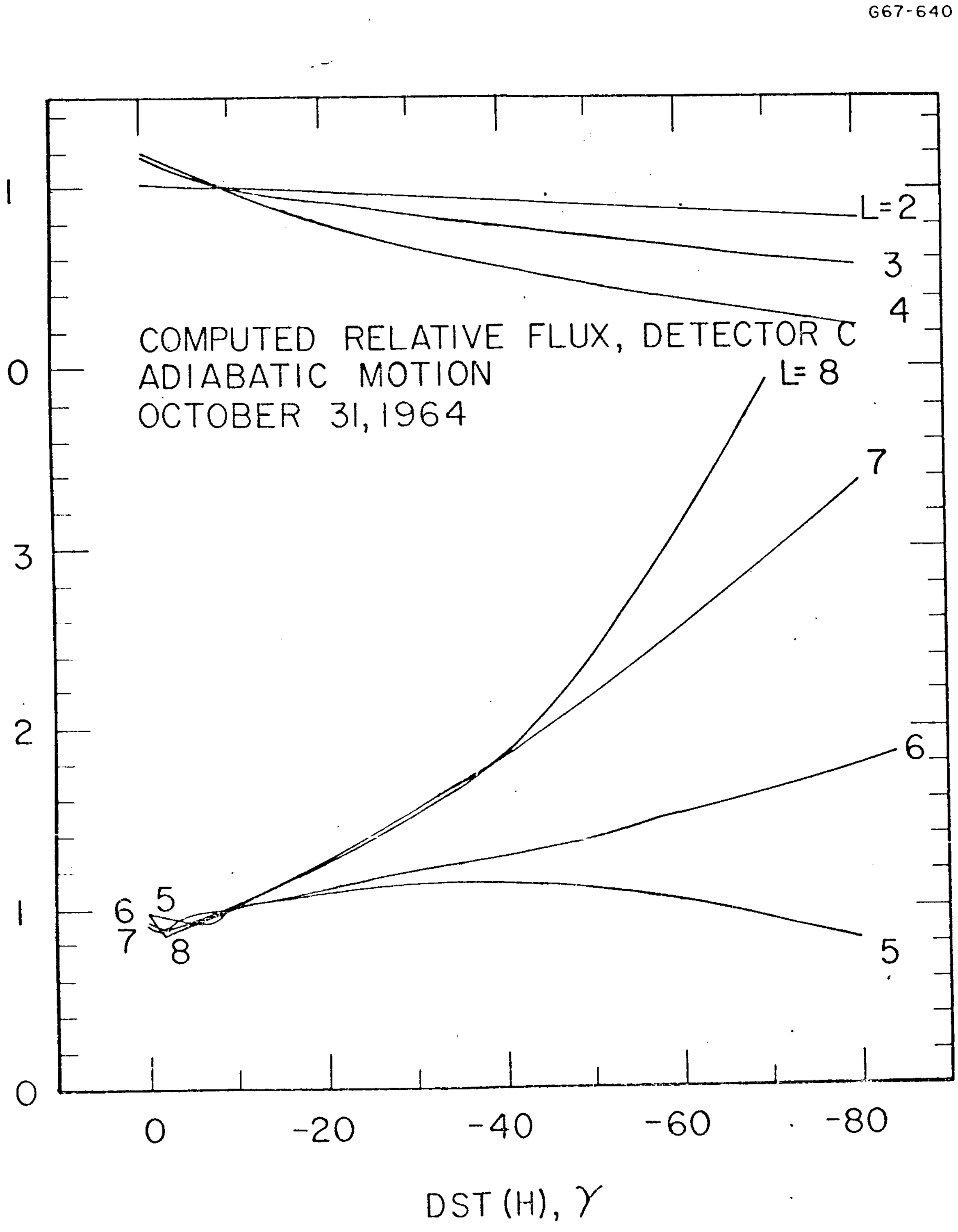
G67-640
COMPUTED RELATIVE FLUX, DETECTOR C
ADIABATIC MOTION
OCTOBER 31, 1964
L=2
3
4
L=8
7
6
5
6
5
7
8
1
0
3
2
1
0
0
-20
-40
-60
-80
DST (H), γ

FIGURE 19

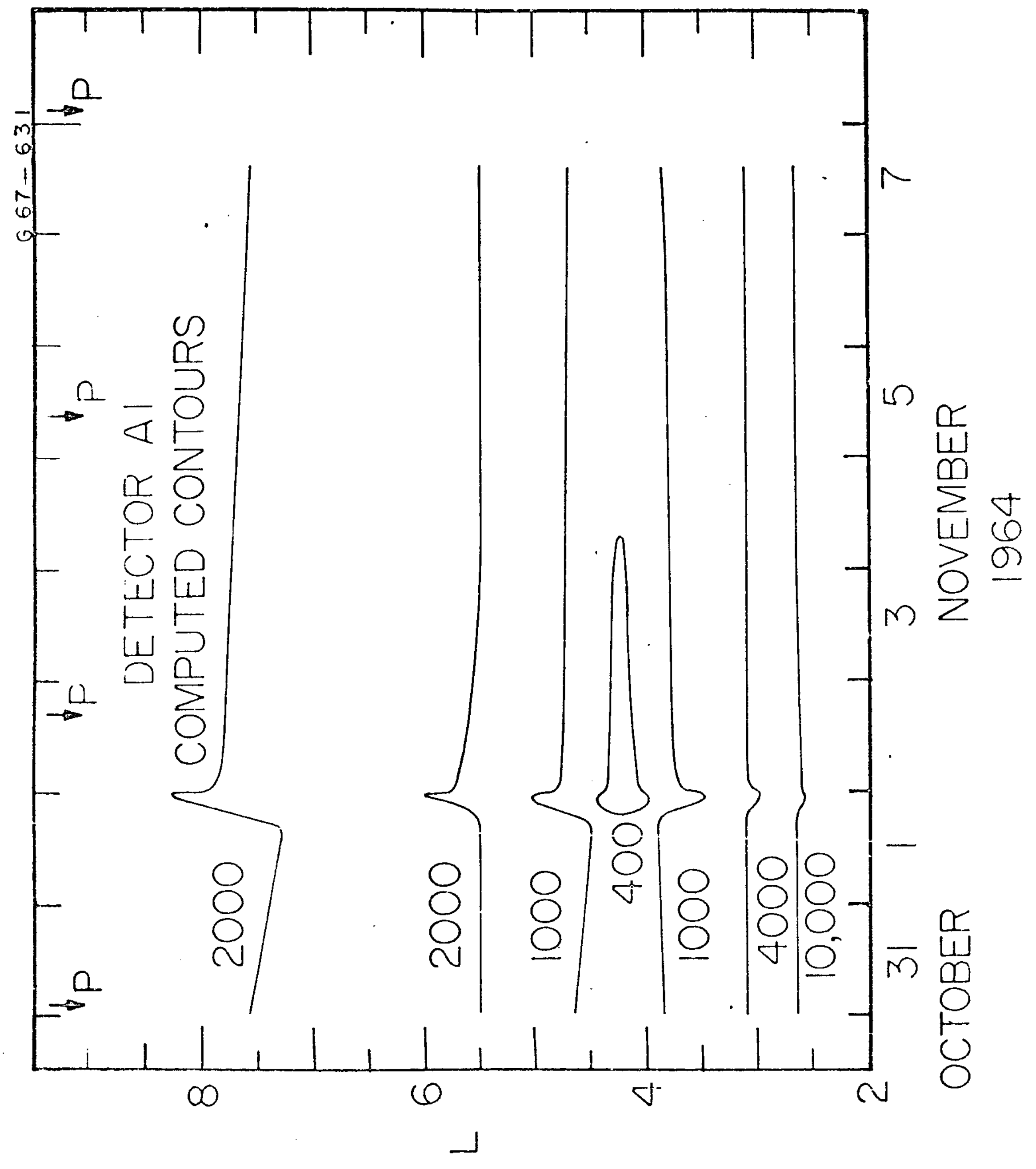
DETECTOR A1
COMPUTED CONTOURS
G 67—631
P
P
P
P
2000
2000
1000
400
1000
4000
10,000
L
8
6
4
2
31
1
3
5
7
OCTOBER
NOVEMBER
1964

FIGURE 20

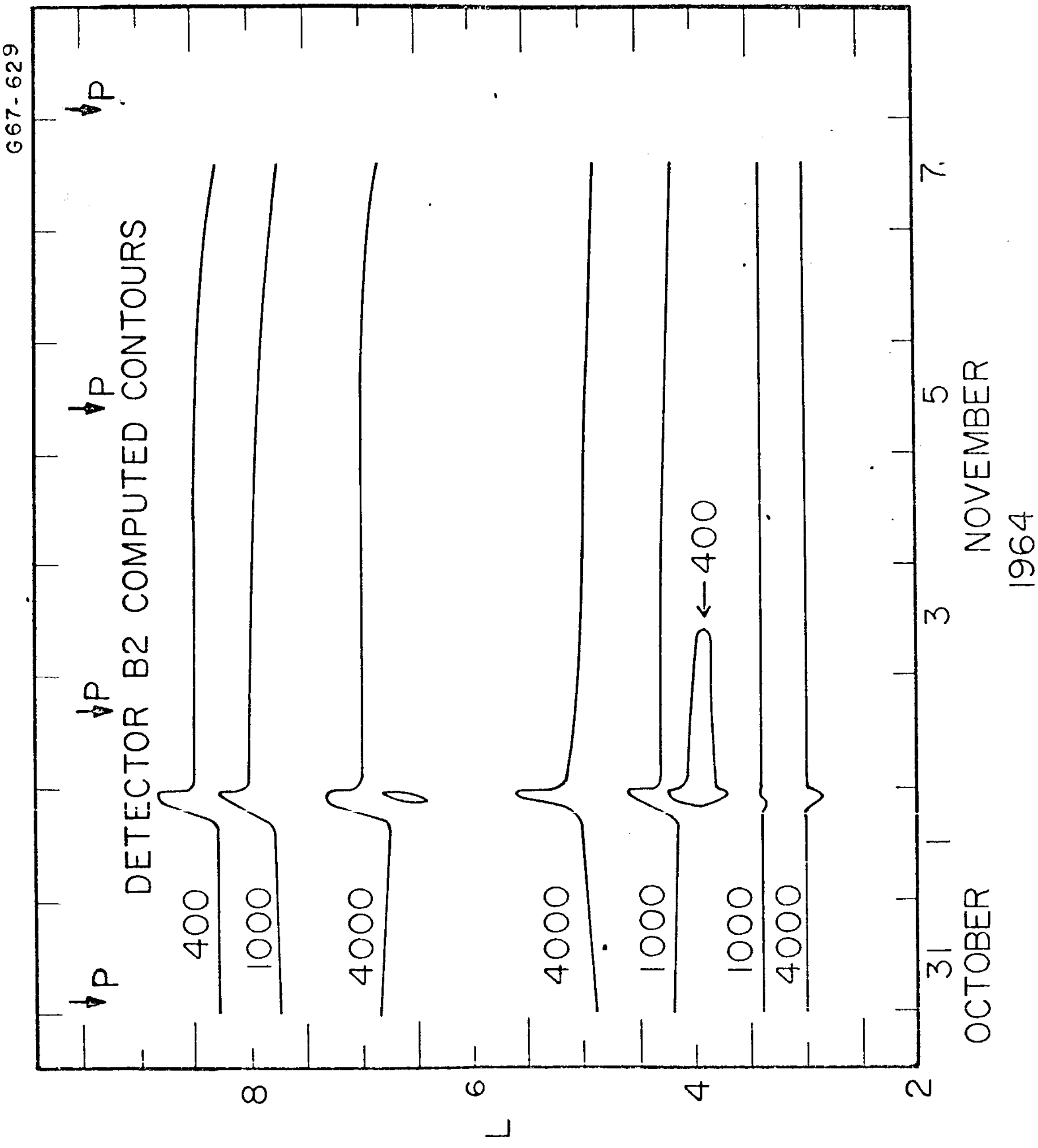
G67-629
DETECTOR B2 COMPUTED CONTOURS
P
P
P
P
400
1000
4000
4000
1000
1000
4000
←400
8
6
4
2
L
31
3
5
7
OCTOBER
NOVEMBER
1964

FIGURE 21

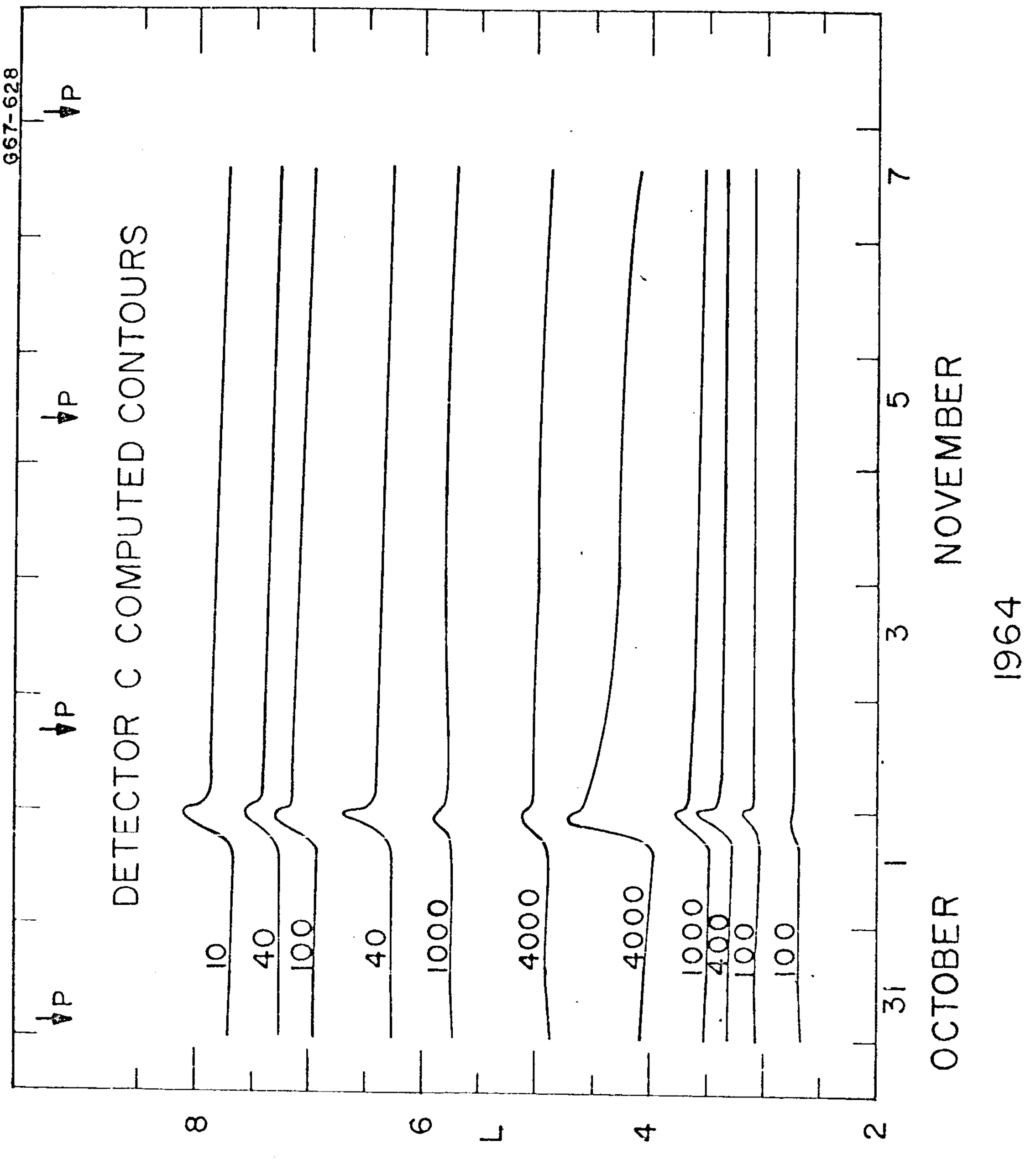
G67-628
DETECTOR C COMPUTED CONTOURS
P
P
P
P
10
40
100
40
1000
4000
4000
1000
400
100
100
8
6
L
4
2
31
1
3
5
7
OCTOBER
NOVEMBER
1964

FIGURE 22

G67-107

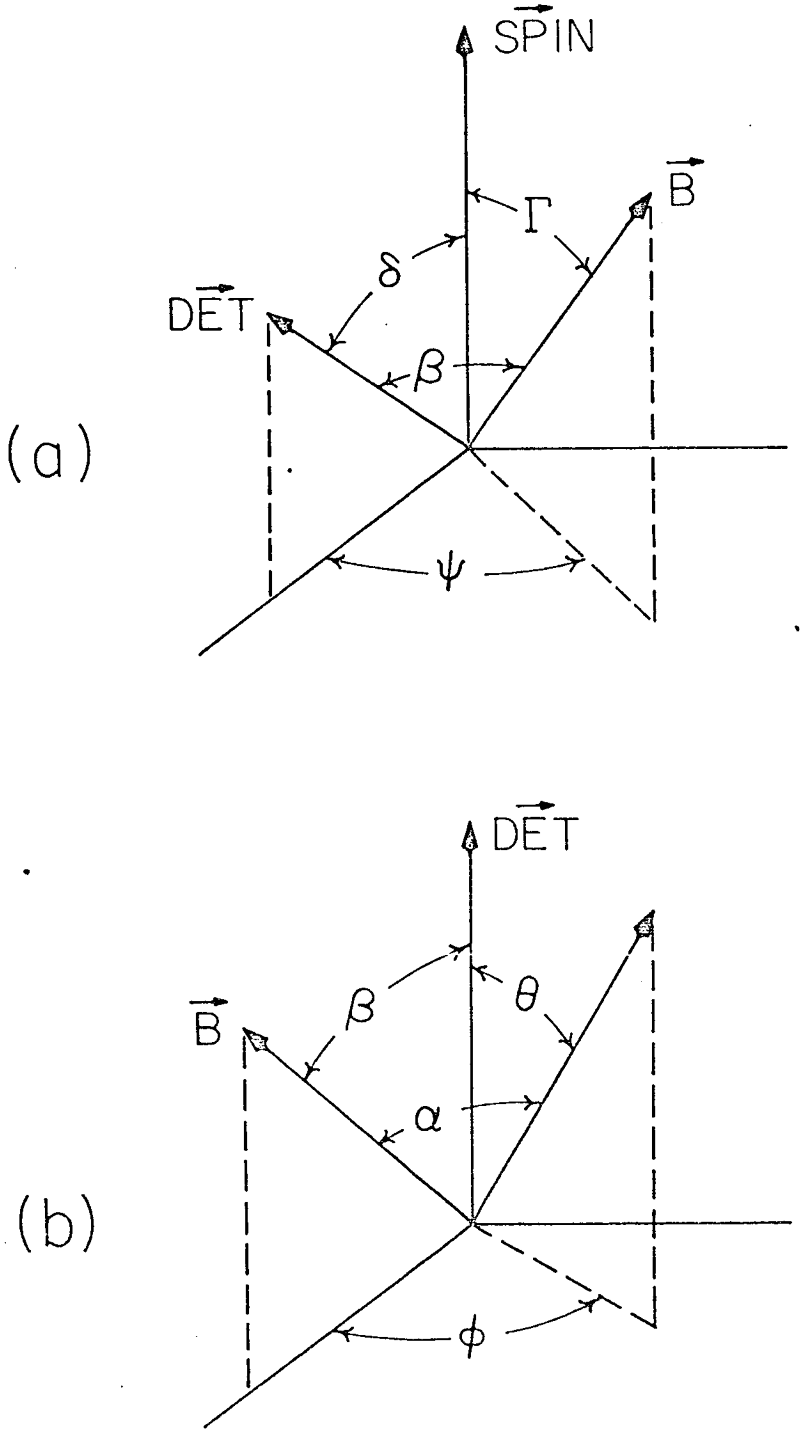

FIGURE 23

G66-882

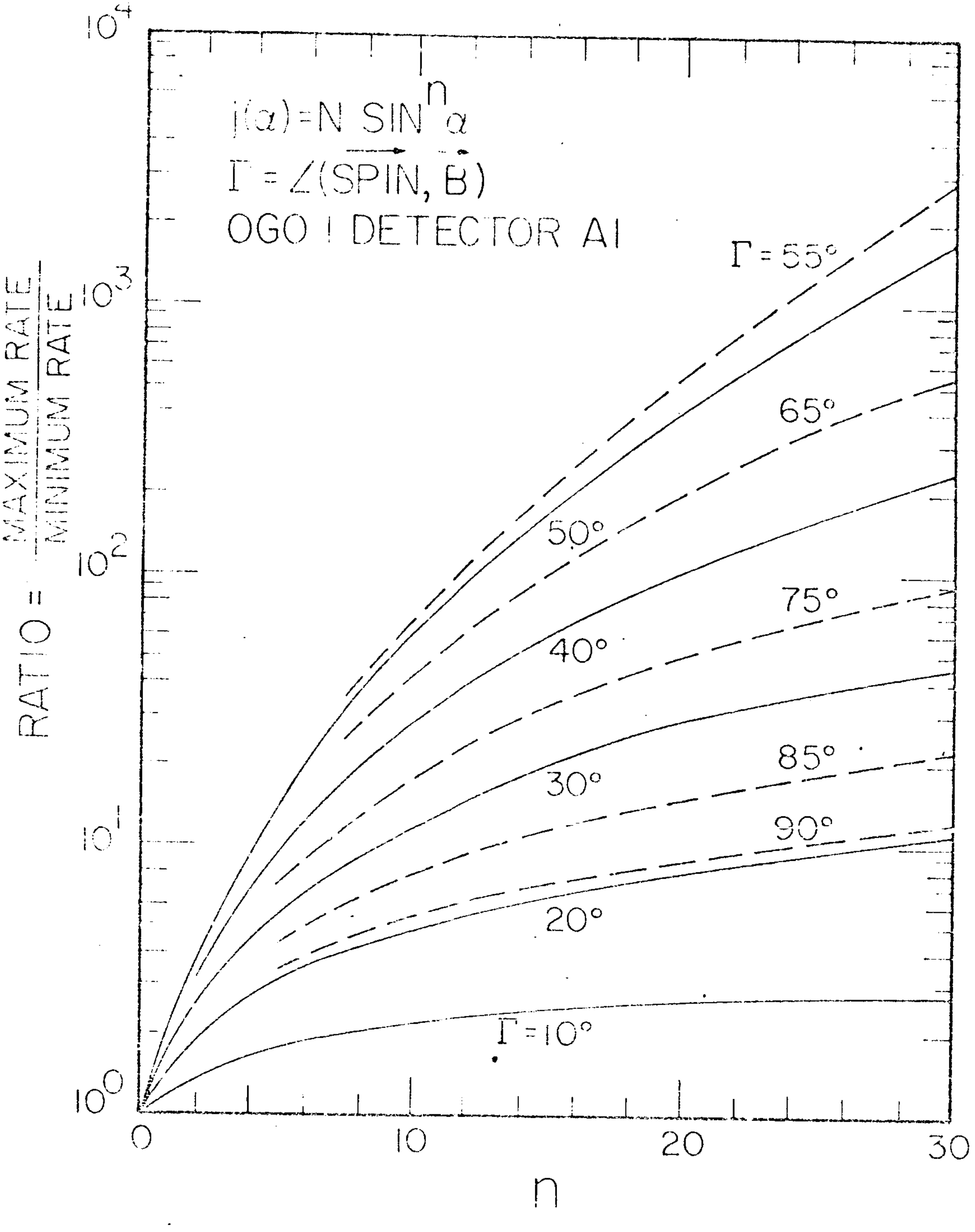

FIGURE 24

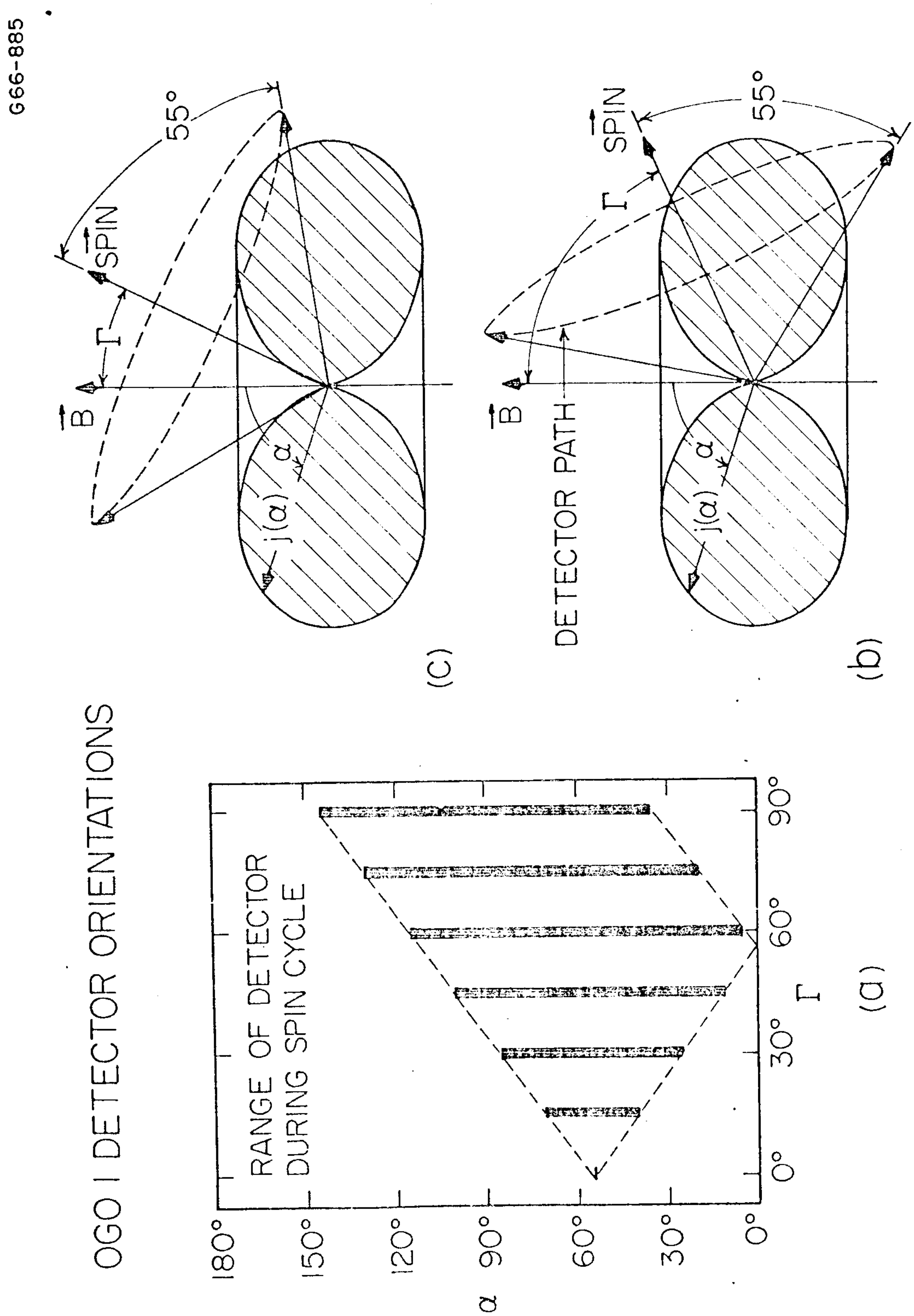

OGO I DETECTOR ORIENTATIONS

FIGURE 25

G67-403

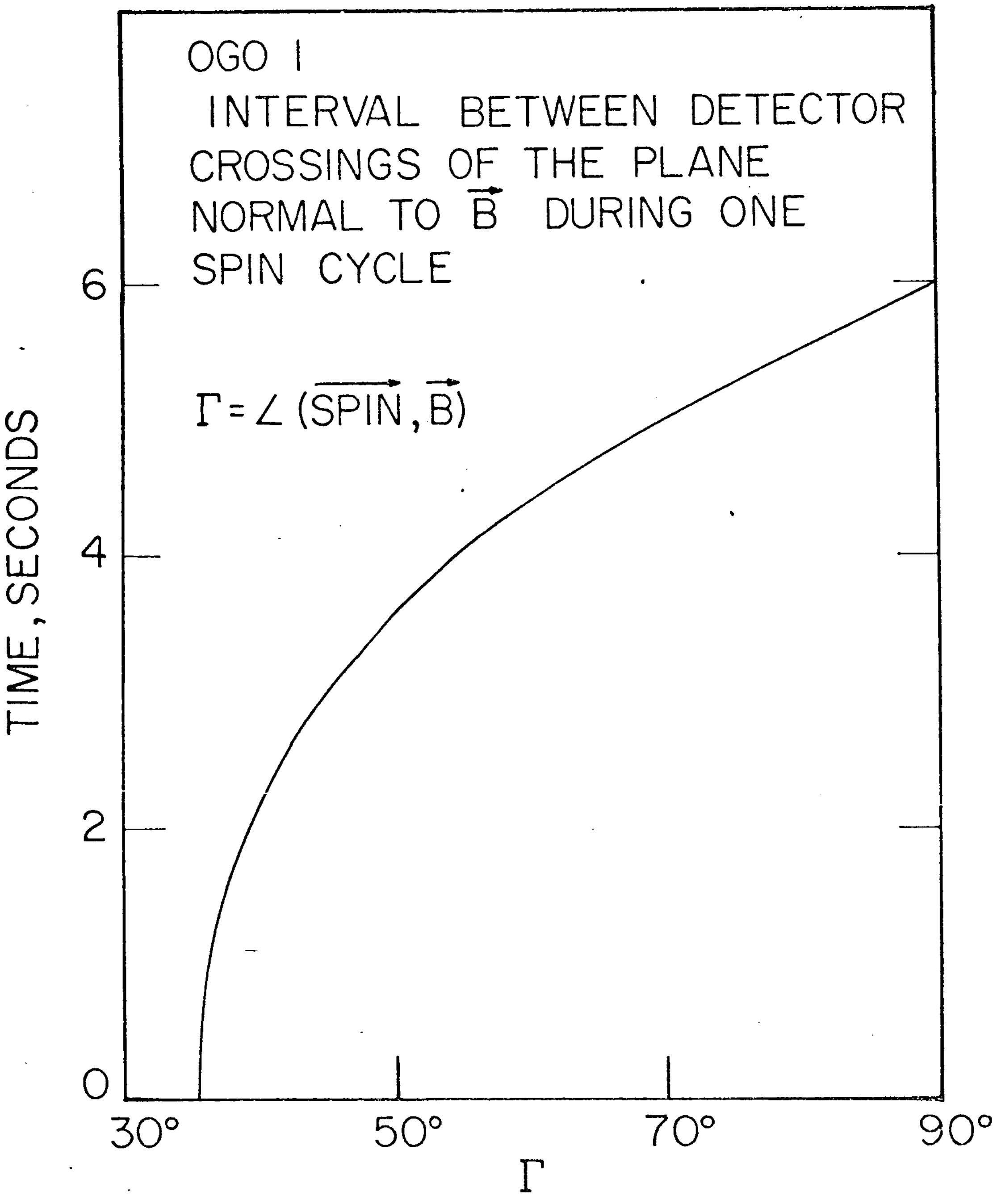

FIGURE 26

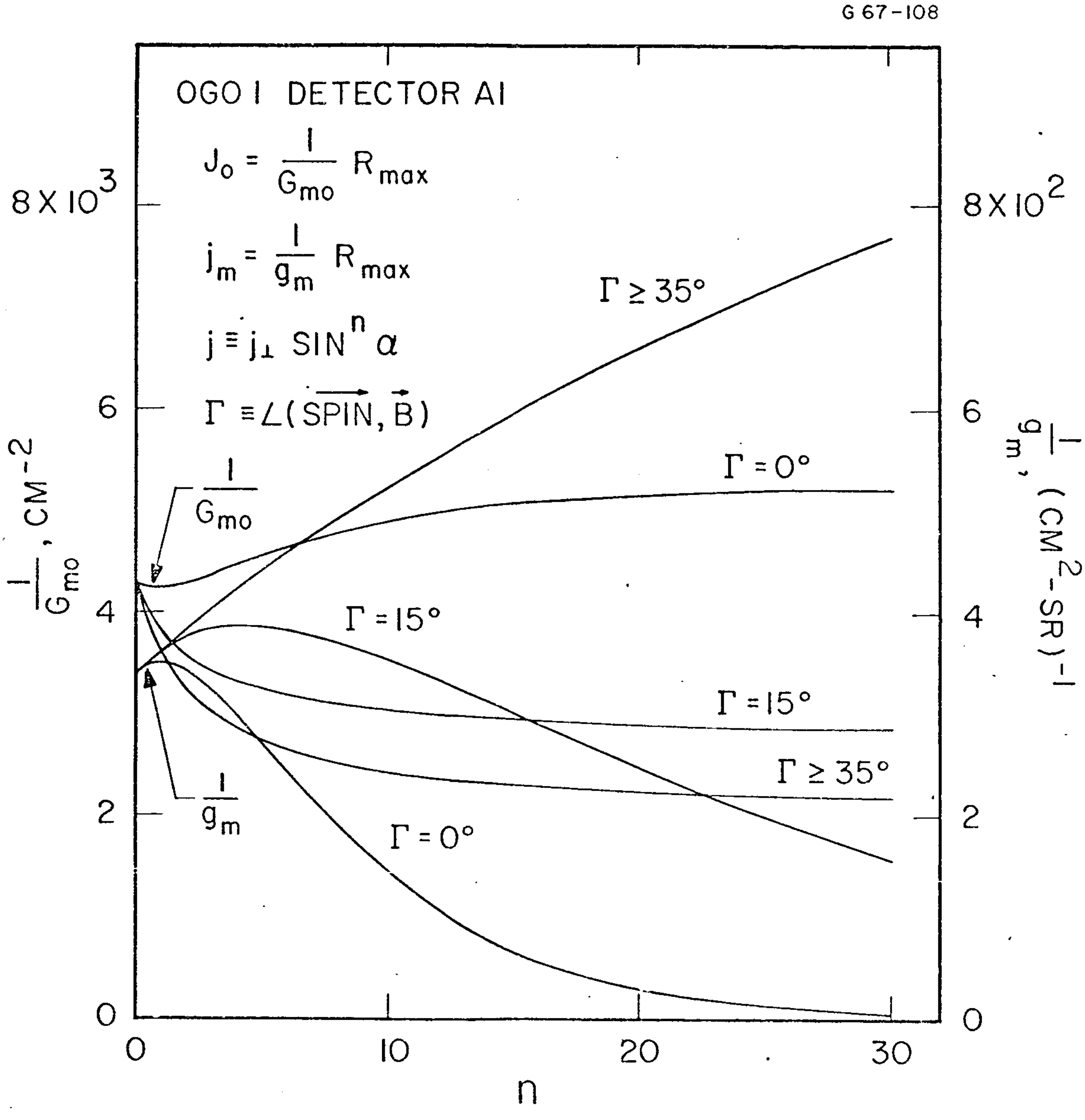
G 67-108
OGO I DETECTOR A1
$J_o = \frac{1}{G_{mo}} R_{max}$
$j_m = \frac{1}{g_m} R_{max}$
$j \equiv j_\perp \sin^n \alpha$
$\Gamma \equiv \angle(\overrightarrow{SPIN}, \vec{B})$
$\frac{1}{G_{mo}}$
$\frac{1}{g_m}$
$\Gamma \geq 35°$
$\Gamma = 0°$
$\Gamma = 15°$
$\Gamma = 15°$
$\Gamma \geq 35°$
$\Gamma = 0°$
$\frac{1}{G_{mo}}$, CM^{-2}
$\frac{1}{g_m}$, (CM^2-SR)$^{-1}$
8×10^3
6
4
2
0
8×10^2
6
4
2
0
0
10
20
30
n

FIGURE 27

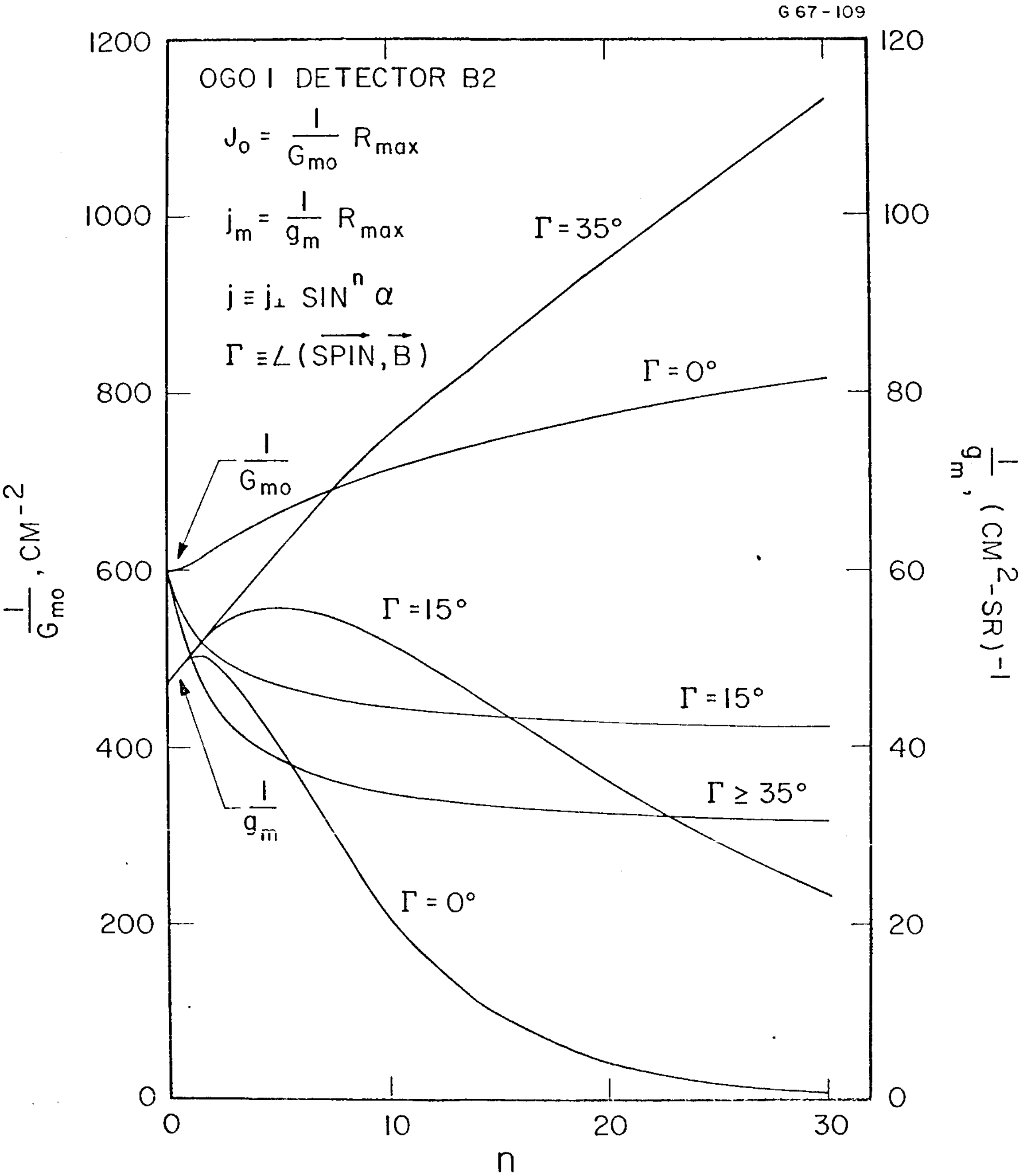
G 67 - 109
OGO I DETECTOR B2
$J_o = \frac{1}{G_{mo}} R_{max}$
$j_m = \frac{1}{g_m} R_{max}$
$j \equiv j_\perp \sin^n \alpha$
$\Gamma \equiv \angle(\overrightarrow{SPIN}, \overrightarrow{B})$
Γ = 35°
Γ = 0°
Γ = 15°
Γ = 15°
Γ ≥ 35°
Γ = 0°
$\frac{1}{G_{mo}}$
$\frac{1}{g_m}$
$\frac{1}{G_{mo}}$, CM^{-2}
$\frac{1}{g_m}$, (CM^2-SR)$^{-1}$
0
200
400
600
800
1000
1200
0
20
40
60
80
100
120
0
10
20
30
n

FIGURE 28

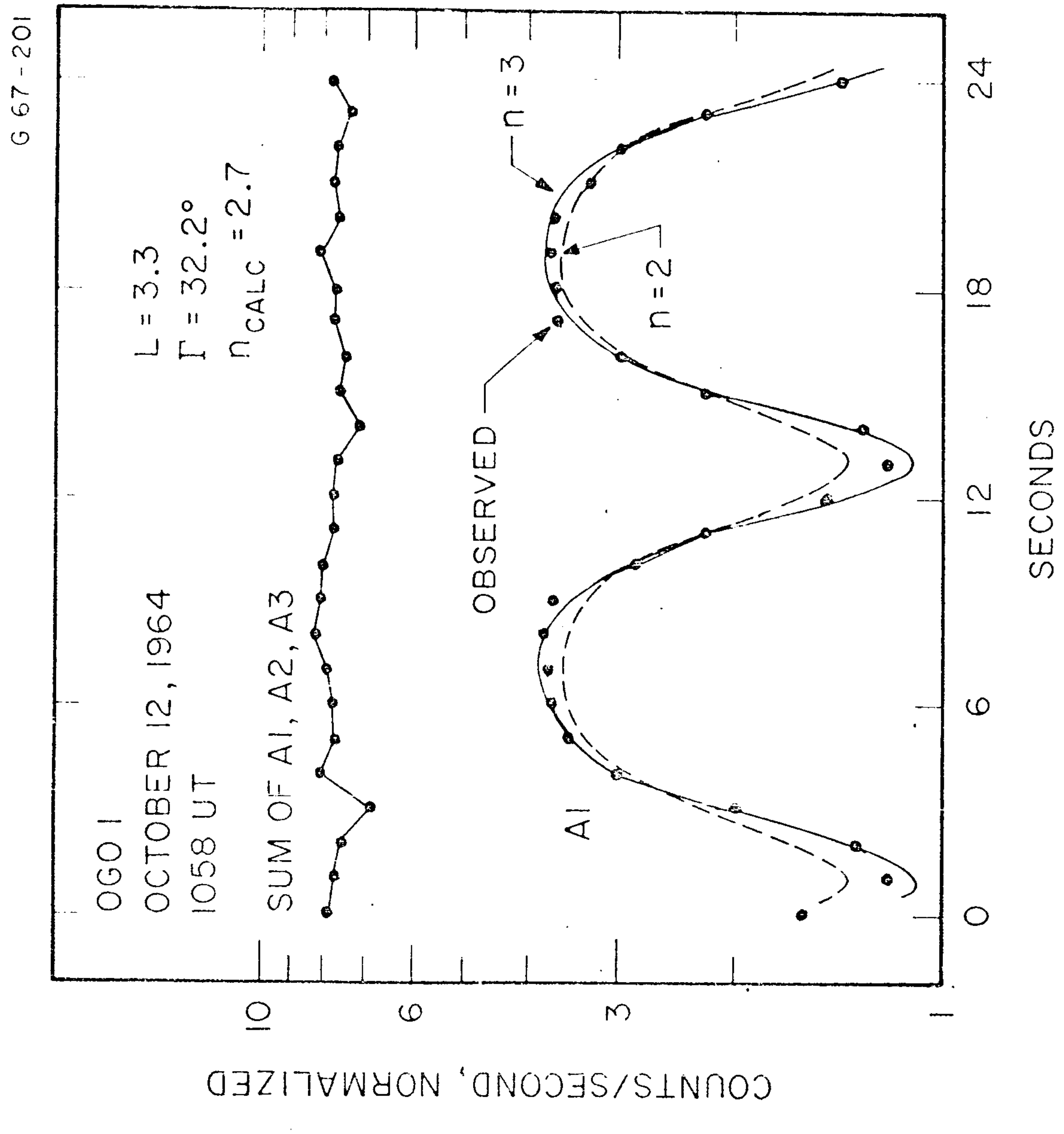
G 67-201
OGO I
OCTOBER 12, 1964
1058 UT
SUM OF A1, A2, A3
A1
L = 3.3
Γ = 32.2°
n_CALC = 2.7
OBSERVED
n = 3
n = 2
0
6
12
18
24
SECONDS
10
6
3
1
COUNTS/SECOND, NORMALIZED

FIGURE 29